

**Noname manuscript No.**  
(will be inserted by the editor)

# Joint Optimization of an Autoencoder for Clustering and Embedding

Ahcène Boubekki · Michael Kampffmeyer ·  
Ulf Brefeld · Robert Jenssen

Received: date / Accepted: date

**Abstract** Incorporating  $k$ -means-like clustering techniques into (deep) autoencoders constitutes an interesting idea as the clustering may exploit the learned similarities in the embedding to compute a non-linear grouping of data at-hand. Unfortunately, the resulting contributions are often limited by ad-hoc choices, decoupled optimization problems and other issues. We present a theoretically-driven deep clustering approach that does not suffer from these limitations and allows for joint optimization of clustering and embedding. The network in its simplest form is derived from a Gaussian mixture model and can be incorporated seamlessly into deep autoencoders for state-of-the-art performance.

**Keywords** Clustering · Deep autoencoders ·  $k$ -means · Gaussian mixture models

## 1 Introduction

Clustering is one of the oldest and most difficult problems in machine learning and a great deal of different clustering techniques have been proposed in the literature. Perhaps the most prominent clustering approach is the  $k$ -means algorithm [31]. Its simplicity renders the application of  $k$ -means particularly attractive to practitioners beyond the field of data mining and machine learning [38, 15, 20, 14].

The model behind the algorithm is also well understood [28, 32] and serves as a basis for a variety of related algorithms and extensions [11, 25, 10]. Nevertheless,  $k$ -means suffers from two main limitations. First, the expressivity is restricted to only linear partitions of the input space due to isotropic cluster assumptions on

---

A. Boubekki  
UiT The Arctic University of Norway, Tromsø, Norway  
E-mail: ahcene.boubekki@uit.no

M. Kampffmeyer  
UiT The Arctic University of Norway, Tromsø, Norway

U. Brefeld  
Leuphana University of Lüneburg, Lüneburg, Germany

R. Jenssen  
UiT The Arctic University of Norway, Tromsø, Norway

the data. Second, similar to other Expectation Maximization variants,  $k$ -means is likely affected by the curse of dimensionality [40] and often underperforms on complex and high dimensional data.

A recent line of research aims to alleviate these issues by learning an embedding of the data with a deep autoencoder (DAE) and to have  $k$ -means operate on the embedded instances [42, 43, 17]. Since the computation of the embedding is (highly) non-linear, the linear solution of  $k$ -means translates to a non-linear solution in input space. This approach resembles the rationale behind kernel methods [18]. The difference between the two approaches lies in either computing a kernel matrix before learning the clustering versus learning the feature map as the function approximated by the encoder. Another advantage of the latter approach is the decoder of the network that allows to map the centroids back into (an approximated version of the) input space. Depending on the kernel function/matrix, this is not always possible with traditional approaches.

However, despite all advantages, how to learn a reversible embedding that also features a  $k$ -means-like clustering objective is still an open question. Existing approaches compute groupings by shrinking the clusters in the embedded space around their centroids. They rely on ad-hoc approaches by devising two (rather independent) optimization problems that, if at all, benefit only partially from one another [42, 43, 17]. Shrinking, in particular, turns out crucial in cases where information is not appropriately shared with the clustering component and may lead to an adaptation of the clustering to the embedding instead of the desired clustering-induced embedding. In general, these approaches cannot handle a random initialization usually leading to noisy embeddings and, in turn, meaningless clusterings.

In this paper, we present a deep clustering approach that avoids these limitations by simultaneously optimizing both the embedding and the clustering. Since deep learning intrinsically relies on gradient descent (GD), we discard the idea of hard,  $k$ -means-like clusterings and resort to isotropic Gaussian mixture models (GMM) [32] as an approximation thereof. We show that the objective function can be translated into a form that allows for GD optimization such that an autoencoder learns the posterior probability of the cluster parameters given the data. The resulting *clustering module* (CM) constitutes the smallest network instance of this approach and we show empirically that it performs comparable to  $k$ -means. However, the solution also shares the same limitations as  $k$ -means. One of the benefits of our contribution lies in its seamless integration into deep autoencoders to learn the coveted reversible feature map *and* the clustering in a joint optimization. The resulting *clustering networks* (C-Nets) constitutes a novel class of architectures and we provide empirical results that exhibit its state-of-the-art performance.

The reminder of the paper is organized as follows. Section 2 reviews related work and Section 3 provides the theory underpinning our contribution. The clustering module (CM) and the deep clustering networks (C-Nets) are presented in Sections 4 and 5, respectively, where we also report the empirical results. Section 6 concludes the paper.

## 2 Related Work

Recently, several deep learning models have been proposed to group data in an unsupervised manner [39, 44, 23, 16, 19, 34, 36]. Among these, one particularly popular direction, which our contribution falls within, aims to learn  $k$ -means friendly embeddings [42, 17, 43, 13]. In this section, we review the most related approaches within this direction.

One of the first approaches to deep clustering is DEC [42], which consists of an embedding network followed by an ad-hoc matrix representing the centroids. During training, the model is trained to shrink the data around their closest centroids in a way similar to t-SNE [33]. However, instead of matching the distributions in the input and feature spaces, a mixture of Student-t models is fitted to the one deriving from a  $k$ -means clustering of the embedding itself. The latter is updated every few iterations to keep track of evolution of the embedding. In order to avoid sub-optimal solutions when starting from randomly initialization, the embedding network is pre-trained as a DAE. However, the difference between the two training phases can cause stability issues, such as collapsing centroids. IDEC [17] extends DEC alleviates this issue by using the reconstruction loss of the DAE also during the training phase. Although IDEC outperforms DEC, both are highly dependent on the initial clustering as the data is shrunk quickly around their centroids.

The Deep Clustering Network (DCN) [43] is based on an architecture comparable to DEC and IDEC but includes hard clustering. The optimization scheme consists of three steps: 1) Optimize the DAE to reconstruct and bring the data-points closer to their closest centroids (similar to  $k$ -means); 2) update assignments to the closest clusters; 3) update iteratively the centroids using the assignments. Although alternating optimization helps prevent instabilities during the optimization, DCN still requires initialization schemes in order to reach good solutions.

Contrary to the other baselines, DKM [13] jointly optimizes a DAE and an ad-hoc matrix representing the centroids. The loss function of the DAE includes a term similar to the loss of fuzzy  $c$ -means [6], i.e,  $k$ -means with soft-assignments. The cluster coefficients are computed from the distances to the centroids and normalized using a parameterized softmax. In order to convert soft assignments into hard ones, the parameter follows an annealing strategy.

Our proposed model instead, while being theoretically-driven, resolves the need for alternative optimization schemes as well as reduces the reliance on pre-training schemes.

## 3 Deriving the objective function

In general, the  $k$ -means algorithm learns a crude and degenerate variant of a Gaussian mixture model under the assumptions [28]: (1) null co-variance matrices (yielding a hard clustering) (2) and equally likely clusters. The former is a challenge to our endeavor since it hinders the computation of a gradient, thus prohibiting gradient descent-based optimization. We, instead, circumvent this issue by considering an isotropic GMM where the co-variance matrices are identical and given by a non-null multiple of the identity. We relax the hypothesis further and replace the second assumption with a symmetric Dirichlet prior. That way, instead of imposing a uniform cluster distribution, the optimization can be rather steered toward it.

As we will see, the resulting function can be rewritten to suit gradient-descent optimization and in particular an autoencoder, paving the way for a neural network approximation of  $k$ -means.

### 3.1 Preliminaries

Throughout the paper the set of positive integers is denoted by  $\mathbb{N}^*$ . The set of the  $d$ -dimensional stochastic vectors is written as  $\mathbb{S}^d = \{\mathbf{x} \in \mathbb{R}_{\geq 0}^d : \sum_{i=1}^d x_i = 1\}$ . When the context allows, the ranges of the indices are abbreviated using the upper-bound, e.g., a vector  $\mathbf{x} \in \mathbb{R}^d$  decomposes as  $\mathbf{x} = \langle x_j \rangle_{1 \leq j \leq d} = \langle x_j \rangle_d$ . The zero vector of  $\mathbb{R}^d$  is written as  $\mathbf{0}_d$ . The notation extends to any number. The identity matrix of  $\mathbb{R}^{d \times d}$  is denoted by  $\mathbf{I}_d$ .

We aim to cluster a data-set  $\mathcal{X} = \{\mathbf{x}_i\}_N \subset \mathbb{R}^d$  consisting of  $N \in \mathbb{N}^*$  *i.i.d.* observations using a Gaussian mixture model with  $K \in \mathbb{N}^*$  components. The set  $\mathcal{Z} = \{z_i\}_N$  aggregates the assignments. The centroids and co-variances are summarized in matrices  $\boldsymbol{\mu} = \langle \boldsymbol{\mu}_k \rangle_K \in \mathbb{R}^{K \times d}$ ,  $\boldsymbol{\Sigma} = \langle \boldsymbol{\Sigma}_k \rangle_K \in \mathbb{R}^{K \times d \times d}$ , respectively. The mixture weights form the stochastic vector

$$\boldsymbol{\Phi} = \langle \phi_k := p(z = k) \rangle_K \in \mathbb{S}^K$$

and the responsibility of cluster  $k$  on a data-point  $\mathbf{x}_i$ , or posterior probability of  $z_i = k$ , is given by the conditional  $\gamma_{ik} := p(z_i = k | \mathbf{x}_i)$ . The vector formed of the cluster responsibilities on  $\mathbf{x}_i$  is the stochastic vector  $\boldsymbol{\gamma}_i \in \mathbb{S}^K$ , as well as the  $i$ -th row of matrix  $\boldsymbol{\Gamma} = \langle \gamma_{ik} \rangle_{N \times K} \in \mathbb{R}^{N \times K}$ . The average responsibility of cluster  $k$  is  $\tilde{\gamma}_k = \frac{1}{N} \sum_{i=1}^N \gamma_{ik}$ .

The usual approach to learn a GMM is to maximize the *expected value of the complete-data log-likelihood* function of the model, also called the  $\mathcal{Q}$ -function [7]:

$$\begin{aligned} \mathcal{Q}(\boldsymbol{\Gamma}, \boldsymbol{\Phi}, \boldsymbol{\mu}, \boldsymbol{\Sigma}) &= \mathbb{E}_{\mathcal{Z}} [\log p(\mathcal{X}, \mathcal{Z} | \boldsymbol{\mu}, \boldsymbol{\Sigma})] \\ &= \sum_{i=1}^N \sum_{k=1}^K p(z_i = k | \mathbf{x}_i) \log [p(z_i = k) \mathcal{N}(\boldsymbol{\mu}_k, \boldsymbol{\Sigma}_k)(\mathbf{x}_i)] \\ &= \sum_{i=1}^N \sum_{k=1}^K \gamma_{ik} \log \phi_k - \frac{1}{2} \gamma_{ik} \log \det \boldsymbol{\Sigma}_k \\ &\quad + \frac{1}{2} \gamma_{ik} (\mathbf{x}_i - \boldsymbol{\mu}_k)^T \boldsymbol{\Sigma}_k^{-1} (\mathbf{x}_i - \boldsymbol{\mu}_k) + \text{constant.} \end{aligned} \tag{1}$$

The Expectation-Maximization algorithm [9] is the standard optimization scheme for a GMM. It alternates until convergence between estimating  $\boldsymbol{\Gamma}$  for a given set of parameters  $(\boldsymbol{\Phi}, \boldsymbol{\mu}, \boldsymbol{\Sigma})$  (Expectation) and maximizing the marginals of  $\mathcal{Q}$  assuming  $\boldsymbol{\Gamma}$  fixed (Maximization). The cluster assignments are then decided from the clusters responsibilities:  $z_i = \arg \max_K \gamma_{ik}$ .

### 3.2 Facilitating gradient descent-based optimization

According to [28], the model learned by  $k$ -means can be interpreted as a degenerate GMM with null co-variance matrices and equally likely clusters/components, i.e.,

$\forall k$ ,  $\phi_k = \frac{1}{K}$  and  $\Sigma_k = \mathbf{0}_{K \times K}$ . To have an objective function that lends itself to a gradient descent optimization, we need to relax these assumptions.

Similarly to [32], we assume fixed isotropic co-variance matrices:

$$\forall k \in [1 \dots K], \Sigma_k = \frac{1}{2} \mathbf{I}_d. \quad (2)$$

Beyond avoiding the inversion of matrices, this hypothesis is key to the simplifications of the following derivations. This is a strong constraint that we aim to alleviate with the DAE embedding.

The second hypothesis of  $k$ -means affects the cluster assignments. Since the latter derive from the  $\gamma_{ik}$ , we assume instead a Dirichlet prior (with parameter  $\alpha \in \mathbb{R}^K \setminus \{\mathbf{0}_K\}$ ) on the average responsibilities:

$$\mathcal{Q}(\boldsymbol{\Gamma}, \boldsymbol{\Phi}, \boldsymbol{\mu}) = \sum_{i=1}^N \sum_{k=1}^K \gamma_{ik} (\log \phi_k - \|\mathbf{x}_i - \boldsymbol{\mu}_k\|^2) + \sum_{k=1}^K (\alpha_k - 1) \log \tilde{\gamma}_k \quad (3)$$

If the prior is symmetric, i.e.,  $\forall k, \alpha_k = \alpha_1 > 0$ , the optimization will steer  $\langle \tilde{\gamma}_k \rangle_K$  as well as  $\boldsymbol{\Phi}$  toward the uniform cluster distribution.

We introduce now an algorithmic trick to make a GD optimization straightforward. The rationale is that both  $\boldsymbol{\Phi}$  and  $\tilde{\gamma}$  influence the assignments, however they may present diverging behaviors. The former governs the average distribution of the data-points across all clusters while the latter decides for a single data-point. To avoid this redundancy and contradicting marginal gradients, we propose to merge them. More precisely, we suppose that we start our derivations after a Maximization step of the EM algorithm when the mixture weights are equal to the average cluster responsibilities:

$$\phi_k = \frac{1}{N} \sum_{i=1}^N \gamma_{ik} = \tilde{\gamma}_k. \quad (4)$$

At this stage, the  $\mathcal{Q}$ -function can be rewritten, up to a constant, as follows:

$$\mathcal{Q}(\boldsymbol{\Gamma}, \boldsymbol{\mu}) = \sum_{i=1}^N \sum_{k=1}^K \gamma_{ik} \log \tilde{\gamma}_k - \sum_{i=1}^N \sum_{k=1}^K \gamma_{ik} \|\mathbf{x}_i - \boldsymbol{\mu}_k\|^2 + \sum_{k=1}^K (\alpha_k - 1) \log \tilde{\gamma}_k \quad (5)$$

A consequence of this computational trick is that the objective function is not equal anymore to the expected value of the complete-data log-likelihood of the model. However, they stay related: at any time the gradient descent can be interrupted;  $\boldsymbol{\Gamma}$  is untied from  $\boldsymbol{\Phi}$  and updated according to the Expectation step, after which the  $\mathcal{Q}$ -function is equal to the complete-data log-likelihood of the model (see [9]).

Since the objective function increases after an E-step, if the gradient descent improves Equation 5, the expected value of complete-data log-likelihood also increases. Assuming the latter bounded, an always improving gradient-based optimization of Equation 5 converges as well.

Note that Equation 5 can be further simplified. The first term corresponds to the entropy  $H$  of  $\tilde{\gamma} = \langle \tilde{\gamma}_k \rangle_K$  which, given the Dirichlet prior, is a function  $F$  of  $\alpha$ :

$$\sum_{i=1}^N \sum_{k=1}^K \gamma_{ik} \log \tilde{\gamma}_k = N \sum_{k=1}^K \tilde{\gamma}_k \log \tilde{\gamma}_k = -NH(\tilde{\gamma}) = F(\alpha),$$

This term is constant with respect to the parameters of the model and is therefore omitted from now on.

$$\mathcal{Q}(\boldsymbol{\Gamma}, \boldsymbol{\mu}) = - \sum_{i=1}^N \sum_{k=1}^K \gamma_{ik} \|\boldsymbol{x}_i - \boldsymbol{\mu}_k\|^2 + \sum_{k=1}^K (\alpha_k - 1) \log \tilde{\gamma}_k \quad (6)$$

The objective function has now two terms and its gradient is well defined.

$$\begin{aligned} \nabla_{\boldsymbol{\mu}_k} \mathcal{Q}(\boldsymbol{v}) &= \sum_{i=1}^N \gamma_{ik} (\boldsymbol{x}_i - \boldsymbol{\mu}_k) \cdot \boldsymbol{v} \\ \frac{\partial \mathcal{Q}}{\partial \gamma_{ik}} &= \|\boldsymbol{x}_i - \boldsymbol{\mu}_k\|^2 + \frac{\alpha_k - 1}{N \tilde{\gamma}_k} \end{aligned} \quad (7)$$

Nonetheless, we decide to go further and expand  $\gamma_{ik} \|\boldsymbol{x}_i - \boldsymbol{\mu}_k\|^2$  in order to gain insight into the mechanics behind the clustering.

### 3.3 Paving the way toward autoencoders

The clustering term  $\gamma_{ik} \|\boldsymbol{x}_i - \boldsymbol{\mu}_k\|^2$  can be expanded by adding and subtracting the norm of  $\bar{\boldsymbol{x}}_i = \sum_{k=1}^K \gamma_{ik} \boldsymbol{\mu}_k$ : For any given  $i \in [1 \dots N]$ ,

$$\begin{aligned} \sum_{k=1}^K \gamma_{ik} \|\boldsymbol{x}_i - \boldsymbol{\mu}_k\|^2 &= \sum_{k=1}^K \gamma_{ik} \|\boldsymbol{x}_i\|^2 - 2\boldsymbol{x}_i^\top \left( \sum_{k=1}^K \gamma_{ik} \boldsymbol{\mu}_k \right) + \sum_{k=1}^K \gamma_{ik} \|\boldsymbol{\mu}_k\|^2 \\ &\quad + \|\bar{\boldsymbol{x}}_i\|^2 - \|\bar{\boldsymbol{x}}_i\|^2 \\ &= \|\boldsymbol{x}_i\|^2 - 2\boldsymbol{x}_i^\top \bar{\boldsymbol{x}}_i + \|\bar{\boldsymbol{x}}_i\|^2 \\ &\quad + \sum_{k=1}^K \gamma_{ik} \|\boldsymbol{\mu}_k\|^2 - \sum_{k=1}^K \sum_{l=1}^K \gamma_{ik} \gamma_{il} \boldsymbol{\mu}_k^\top \boldsymbol{\mu}_k \\ &= \|\boldsymbol{x}_i - \bar{\boldsymbol{x}}_i\|^2 + \sum_{k=1}^K \gamma_{ik} (1 - \gamma_{ik}) \|\boldsymbol{\mu}_k\|^2 - \sum_{k=1}^K \sum_{\substack{l=1 \\ l \neq k}}^K \gamma_{ik} \gamma_{il} \boldsymbol{\mu}_k^\top \boldsymbol{\mu}_l. \end{aligned}$$

Note that this simplification grounds on the isotropic assumption; it is not obvious how to reach a similar result without isotropy. Finally, the  $\mathcal{Q}$ -function becomes the sum of four terms which we discuss hereafter:

$$\begin{aligned} \mathcal{Q}(\boldsymbol{\Gamma}, \boldsymbol{\mu}) &= - \underbrace{\sum_{i=1}^N \|\boldsymbol{x}_i - \bar{\boldsymbol{x}}_i\|^2}_{=: E_1} - \underbrace{\sum_{i=1}^N \sum_{k=1}^K \gamma_{ik} (1 - \gamma_{ik}) \|\boldsymbol{\mu}_k\|^2}_{=: E_2} \\ &\quad + \underbrace{\sum_{i=1}^N \sum_{k=1}^K \sum_{\substack{l=1 \\ l \neq k}}^K \gamma_{ik} \gamma_{il} \boldsymbol{\mu}_k^\top \boldsymbol{\mu}_l}_{=: E_3} - \underbrace{\sum_{k=1}^K (1 - \alpha_k) \log \tilde{\gamma}_k}_{=: E_4}. \end{aligned} \quad (8)$$

*E<sub>1</sub>: Reconstruction* There are two operations involved to obtain  $\bar{\mathbf{x}}_i$ : the computation of  $\boldsymbol{\gamma}_i$  and the dot-product thereof with  $\boldsymbol{\mu}$ . This can be formalized using two functions  $\mathcal{F}$  and  $\mathcal{G}$  with parameters  $\boldsymbol{\eta}$  and  $\boldsymbol{\mu}$ , respectively, such that:

$$\begin{aligned}\mathcal{F} : \mathbb{R}^d &\rightarrow \mathbb{S}^K \\ \mathbf{x} &\mapsto \mathcal{F}(\mathbf{x}; \boldsymbol{\eta}) = \langle p(z = k | \mathbf{x}) \rangle_K = \boldsymbol{\gamma} \\ \mathcal{G} : \mathbb{S}^K &\rightarrow \mathbb{R}^d \\ \boldsymbol{\gamma} &\mapsto \mathcal{G}(\boldsymbol{\gamma}; \boldsymbol{\mu}) = \sum_{k=1}^K \gamma_k \boldsymbol{\mu}_k = \bar{\mathbf{x}}\end{aligned}\tag{9}$$

Recall that the cluster responsibility  $\gamma_{ik}$  is also the posterior probability of  $z_i$  given  $\mathbf{x}_i$ , i.e.  $\gamma_{ik} = p(z_i = k | \mathbf{x}_i)$ , which is indeed a function of the input.  $E_1$  can thus be stated as:

$$E_1 = \sum_{i=1}^N \|\mathbf{x}_i - \mathcal{G}(\mathcal{F}(\mathbf{x}_i))\|^2.$$

This last equation can be interpreted as the reconstruction loss of an autoencoder such that  $\mathcal{F}$  and  $\mathcal{G}$  are approximated by the encoder and decoder networks, respectively, and  $\boldsymbol{\gamma}$  is the code. The term  $E_1$  suggests thus an autoencoder structure to optimize  $\mathcal{Q}$ .

*E<sub>2</sub>: Sparsity and regularization* The second term  $E_2$  is related to the Gini impurity index [8] applied to  $\boldsymbol{\gamma}_i$ :

$$\sum_{k=1}^K \gamma_{ik} (1 - \gamma_{ik}) \|\boldsymbol{\mu}_k\|^2 \leq \sum_{k=1}^K \gamma_{ik} (1 - \gamma_{ik}) \|\boldsymbol{\mu}\|_F^2 = \mathbf{Gini}(\boldsymbol{\gamma}_i) \|\boldsymbol{\mu}\|_F^2,$$

where  $\|\cdot\|_F$  is the Frobenius norm. The Gini index is standard in decision tree theory to select branching features and is an equivalent of the entropy. It is non-negative and null if, and only if,  $\boldsymbol{\gamma}_i$  is a one-hot vector. Hence, minimizing this term favors sparse  $\boldsymbol{\gamma}_i$  resulting in clearer assignments.

The terms  $\|\boldsymbol{\mu}_k\|^2$  play a role similar to an  $\ell_2$ -regularization: they prevent the centroids from diverging away from the data-points. However, they may also favor the trivial solution where all the centroids are merged into zero.

*E<sub>3</sub>: Sparsity and cluster merging* To study the behavior of  $E_3$  during the optimization, let us consider a simple example with one observation and two clusters, i.e.,  $\boldsymbol{\Gamma} \equiv \boldsymbol{\gamma}_1 = (\gamma, 1 - \gamma)$ . If the observation is unambiguously assigned to one cluster,  $\boldsymbol{\gamma}_1$  is a one-hot vector and  $E_3$  is null. If it is not the case, the difference between  $E_2$  and  $E_3$  factorizes as follows:

$$E_2 - E_3 = \gamma(1 - \gamma)(\|\boldsymbol{\mu}_1\|^2 + \|\boldsymbol{\mu}_2\|^2 - \boldsymbol{\mu}_1^T \boldsymbol{\mu}_2) = \gamma(1 - \gamma) \|\boldsymbol{\mu}_1 - \boldsymbol{\mu}_2\|^2.\tag{10}$$

The optimization will thus either push  $\boldsymbol{\gamma}_1$  toward a more sparse vector, or merge the two centroids. Appendix A.3 presents an analysis of the role of this term.

*E<sub>4</sub>: Balancing* The Dirichlet prior steers the distribution of the cluster assignments. If none of the  $\alpha_k$  is null, the prior will push the optimization to use all the clusters, moderating thus the penchant of *E<sub>2</sub>* for the trivial clustering [43, 17].

Note that if  $\boldsymbol{\alpha} = (1 + \frac{1}{K}) \mathbf{1}_K$ , *E<sub>4</sub>* is, up to a constant, equal to the Kullback-Leibler (KL) divergence between a multinomial distribution with parameter  $\tilde{\boldsymbol{\gamma}}$  and the uniform multinomial distribution:

$$\sum_{k=1}^K (1 - \alpha_k) \log \tilde{\gamma}_k = \sum_{k=1}^K (1 - (1 + \frac{1}{K})) \log \tilde{\gamma}_k = D_{KL} \left( \frac{1}{K} \mathbf{1}_K \middle\| \tilde{\boldsymbol{\gamma}} \right).$$

### 3.4 Intermediate summary

Since we cannot optimize *k*-means itself using gradient descent, we approximate it with a model sharing similar hypotheses, namely an isotropic Gaussian mixture model with a Dirichlet prior. In order to facilitate the optimization and avoid contradicting gradients, we merge  $\boldsymbol{\Phi}$  and  $\boldsymbol{\Gamma}$ . The objective function is not anymore equal to the complete data-likelihood of our model but their growth stays tied. Finally, we broke down the emblematic  $\|\mathbf{x}_i - \boldsymbol{\mu}_k\|^2$ , the main characteristic of *k*-means, into three terms revealing its hidden mechanic. In particular, the final objective function contains a term indicating that the underlying model can be learned using an autoencoder. This is a novel insight on classical *k*-means and GMM that we shall exploit.

## 4 The Clustering Module

In this section, we define the *Clustering Module* as one of the smallest neural networks which can learn our regularized isotropic GMM. After discussing some implementation aspects, we confirm empirically that it matches *k*-means in terms of clustering performance. We also evaluate a model selection based on the sparsity of the assignments. An analysis of the hyper-parameters and of the Dirichlet prior can be found in the Appendix.

### 4.1 Definition

As we have seen, *E<sub>1</sub>* suggests that an autoencoder can optimize Equation 8. This implies a change of paradigm. An EM-based optimization searches, in a real vector space, the parameters  $(\boldsymbol{\Gamma}, \boldsymbol{\mu})$  maximizing that equation, while an autoencoder learns to approximate  $\mathcal{F}$  and  $\mathcal{G}$ , such that  $\boldsymbol{\mu}$  and  $\boldsymbol{\Gamma} = \mathcal{F}(\mathcal{X}; \boldsymbol{\eta})$  are optimal.

According to Equation 9,  $\mathcal{G}$  is the linear function with parameter  $\boldsymbol{\mu}$ . Without loss of generality, we assume an affine function instead and model  $\mathcal{G}$  with a single layer neural network with bias. The centroids remain accessible as the images of the canonical basis of  $\mathbb{R}^K$ . Regarding  $\mathcal{F}$ , the encoder's architecture can be anything as long as it has a stochastic output.

We define the Clustering Module (CM) as the two-layer autocoder, with a single-layer encoder followed by a softmax activation. The operations involved are

formalized as follows:

$$\mathcal{F}(\mathbf{X}) = \text{softmax}(\mathbf{X}\mathbf{W}_{\text{enc}} + \mathbf{B}_{\text{enc}}) = \boldsymbol{\Gamma}$$

$$\mathcal{G}(\boldsymbol{\Gamma}) = \boldsymbol{\Gamma}\mathbf{W}_{\text{dec}} + \mathbf{B}_{\text{dec}} = \bar{\mathbf{X}},$$

for input  $\mathbf{X} \in \mathbb{R}^{N \times d} \sim \mathcal{X}$ , code representation/cluster responsibilities  $\boldsymbol{\Gamma} = \langle \gamma_{ik} \rangle_{N \times K} \in \mathbb{R}^{N \times K}$  s.t.  $\gamma_i \in \mathbb{S}^K$ , and reconstruction  $\bar{\mathbf{X}} \in \mathbb{R}^{N \times d}$ , respectively. The weight and bias parameters for the encoder are  $\mathbf{W}_{\text{enc}} \in \mathbb{R}^{d \times K}$  and  $\mathbf{B}_{\text{enc}} \in \mathbb{R}^K$ , respectively, and analogously for the decoder  $\mathbf{W}_{\text{dec}} \in \mathbb{R}^{K \times d}$  and  $\mathbf{B}_{\text{dec}} \in \mathbb{R}^d$ . The softmax is used as the activation function after the first layer to enforce the code's stochasticity. The centroids  $\boldsymbol{\mu}$  of the underlying GMM correspond to the column-vectors of matrix  $\mathbf{W}_{\text{dec}} + \mathbf{B}_{\text{dec}}$ . The associated loss function is the negative of Equation 8:

$$\begin{aligned} \mathcal{L}_{\text{CM}}(\mathcal{X}; \Theta) = & \sum_{i=1}^N \|\mathbf{x}_i - \bar{\mathbf{x}}_i\|^2 + \sum_{i=1}^N \sum_{k=1}^K \gamma_{ik}(1 - \gamma_{ik}) \|\boldsymbol{\mu}_k\|^2 \\ & - \sum_{i=1}^N \sum_{k=1}^K \sum_{l=1 \atop l \neq k}^K \gamma_{ik} \gamma_{il} \boldsymbol{\mu}_k^T \boldsymbol{\mu}_l + \sum_{k=1}^K (1 - \alpha_k) \log \tilde{\gamma}_k, \end{aligned} \quad (11)$$

with  $\Theta = (\mathbf{W}_{\text{enc}}, \mathbf{B}_{\text{enc}}, \mathbf{W}_{\text{dec}}, \mathbf{B}_{\text{dec}})$ . In case of a batch optimization,  $\tilde{\gamma}$  is computed over the batch.

#### 4.2 Initialization and finalization

Two key aspects of the implementation of a clustering module need to be discussed: the initialization and the computation of the final centroids.

*Initialization* The CM can be initialized using  $k$ -means or any initialization scheme thereof such as  $k$ -means++ [5]. In such a case, the column-vectors of  $\mathbf{W}_{\text{dec}}$  are set equal to the desired centroids. The pseudo-inverse of this matrix becomes the encoder's weights,  $\mathbf{W}_{\text{enc}}$ , and both biases vectors are initialized at null.

*Averaging epoch* In practice, the optimizer updates the positions of the centroids given the current batch. A small batch-size relative to the size of  $\mathcal{X}$  may cause dispersion of the intermediate centroids. Hence, choosing the final centroids based on the last iteration may be sub-optimal.

Let us consider the following toy example to illustrate this phenomenon (Figure 1). The data consists of  $N = 2,000$  points in  $\mathbb{R}^2$  drawn from a mixture of five bivariate Gaussians ( $K = 5$ ) (gray

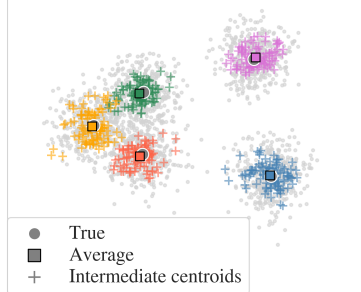


**Fig. 1** The intermediate centroids of the last epoch are spread, whereas their averages almost match the true centroids.

dots). The data is standardized before processing. A CM is trained in mini-batches of size 20 over 50 epochs using stochastic gradient descent. The concentration is set to  $\alpha = 5_K$ .

The dispersion of the centroids after each iteration of the last epoch (crosses) is significant. On the other hand, their average positions (squares) provide a good approximation of the true centers (circles). Therefore, we include one extra epoch to any implementation of CM to compute the average position of the individual centroids over the last iterations.

### 4.3 Empirical evaluation of the clustering module

In this section, we compare empirically the clustering performance of our clustering module and  $k$ -means as a sanity check of the theoretical construction. We also discuss model selection leveraging the ambiguity of the assignments. An analysis of the hyper-parameters and of the Dirichlet prior are reported in Appendix A.1 and A.2, respectively.

#### 4.3.1 Experimental Setting

*Data-sets* We use common benchmark data-sets in the deep clustering literature: MNIST [29], fMNIST [41], USPS [2], CIFAR10 [26], R10K<sup>1</sup>, 20News<sup>2</sup>, 10x73k [45] and Pendigit [4]. They all contains 10 classes except 20News and 10x73k which have 20 and 8 classes, respectively.

*Baselines and implementations* The Clustering Module is implemented using TensorFlow 2.1 [3]<sup>3</sup>. It is optimized over 150 epochs using the Adam [24] optimizer with standard parameters. The Dirichlet prior is symmetric. The size of the mini-batches and  $\alpha$  for each data-set are given in Table 7 of Appendix A.5. We report clustering scores after the averaging epoch.

We used the scikit-learn implementations [37] of  $k$ -means that is run for up to 150 iterations.

*Evaluation metrics* The clustering performance of each model is evaluated using three frequently-used metrics: the Adjusted Rand Index (ARI) [22], the Normalized Mutual Information (NMI) [12] and the clustering accuracy (ACC) [27]. These metrics range between 0 and 1 where the latter indicates perfect clustering. For legibility, values are always multiplied by 100.

#### 4.3.2 Clustering performance

In this experiment, we compare clustering performances and initialization schemes. Since these data-sets are too complex for a linear clustering, we do not expect state-of-the-art results. Random and  $k$ -means++ initialization are indicated with

<sup>1</sup> <https://github.com/XifengGuo/IDEC/files/1613386/usps.zip>

<sup>2</sup> <http://people.csail.mit.edu/jrennie/20Newsgroups>

<sup>3</sup> Code available at:

<https://anonymous.4open.science/r/160597dc-005c-43bd-b5b3-3689e2bac054>

**Table 1** The clustering scores ( $\times 100$ ) of different models on the selected data-sets. The highest score per column and those non-statistically different are marked in boldface. The \* indicate the model with the highest best score.

Model	MNIST			fMNIST			USPS			CIFAR10		
	ARI	NMI	ACC	ARI	NMI	ACC	ARI	NMI	ACC	ARI	NMI	ACC
KM <sup>r</sup>	37.8	<b>49.9*</b>	54.5*	36.6	51.6	53.2	52.6	<b>61.8</b>	63.0	4.2	8.1	20.8
KM <sup>p</sup>	36.9	<b>49.2</b>	54.0	35.2	51.0	50.8	50.2	60.8	61.1	4.2	8.1	20.7
CM <sup>r</sup>	<b>39.7*</b>	<b>50.0</b>	<b>56.8</b>	<b>42.3</b>	<b>54.0</b>	<b>62.0</b>	<b>54.3</b>	<b>62.8</b>	<b>67.0</b>	4.8	8.9	<b>22.0</b>
CM <sup>p</sup>	<b>39.1</b>	<b>49.5</b>	<b>55.9</b>	<b>41.4*</b>	<b>53.4*</b>	<b>60.7*</b>	<b>53.4*</b>	<b>62.8*</b>	<b>63.7*</b>	<b>4.9*</b>	<b>9.3*</b>	<b>22.3*</b>
Model	R10K			20News			10x73k			Pendigit		
	ARI	NMI	ACC	ARI	NMI	ACC	ARI	NMI	ACC	ARI	NMI	ACC
KM <sup>r</sup>	<b>33.8</b>	<b>38.1</b>	<b>61.2</b>	14.8	<b>32.3</b>	<b>31.0</b>	36.5	55.4	55.0	<b>56.5</b>	<b>67.8</b>	<b>71.1</b>
KM <sup>p</sup>	29.5	<b>36.0</b>	58.3	14.8	<b>33.5*</b>	<b>32.0*</b>	36.7	55.5	55.3	<b>58.1</b>	<b>68.9</b>	<b>72.7</b>
CM <sup>r</sup>	<b>38.5</b>	41.0	<b>64.9</b>	9.7	21.2	18.3	<b>54.8</b>	<b>63.8</b>	<b>69.5</b>	<b>57.3</b>	<b>67.0</b>	<b>72.0</b>
CM <sup>p</sup>	<b>32.6*</b>	<b>39.2*</b>	<b>60.2*</b>	<b>16.3*</b>	28.8	<b>30.8</b>	<b>55.4*</b>	<b>64.0*</b>	<b>71.0*</b>	<b>57.3</b>	<b>66.9</b>	<b>72.3</b>

the indices <sup>r</sup> and <sup>p</sup>, respectively. Each experiment is repeated 20 times. We report averages on Table 1. The scores non-statistically significant different from the highest on each data-set ( $p < .05$ ) are marked in boldface. The \* indicate the model with the highest best score. An extended table including standard deviations and best run is can be found in Table 6 of Appendix A.4.

As expected, CM performs similarly and even sometimes better than  $k$ -means on every data-set with respect to almost every metrics and for any initialization scheme. On 10x73k, CM outperforms the baseline model by more than 16 points. Except on 20News,  $k$ -means++ initialization does not significantly improve the results. An analysis of the poor results of CM<sup>r</sup> on this data-set revealed that standardization helps. We did not apply standardization because in average it hinders the performances of the models.

#### 4.3.3 Involving ambiguity for model selection

In an unsupervised scenario, true labels are not available. It is thus necessary to have an internal measure to avoid selecting a sub-optimal solution.

There are two natural choices: select either the clustering associated with the lowest loss or the less ambiguous clustering. In the first case, the sparsity of the clusters responsibilities  $\gamma_i$  might be eclipsed by other aspects optimized by the  $\mathcal{L}_{CM}$ , such as the reconstruction term. On the other hand, by selecting only given the sparsity, we may end up always choosing the most degenerate clustering. As a compromise, we propose to use  $\mathcal{L}_{sp} = E_2 + E_3$  which sums both terms of the loss governing the sparsity of the  $\gamma_i$ s and also involves the norm of the  $\mu_k$ s.

In Table 2, we report the ARI of the runs with the lowest  $\mathcal{L}_{sp}$  for each data-set. For comparison, we also report the average and the largest ARI. Scores selected according to  $\mathcal{L}_{sp}$  that were higher than the average are marked in boldface.

A model selection based on  $\mathcal{L}_{sp}$  finds the best runs only for R10K. Nevertheless, it selects runs with ARI greater than the average in more than half of the cases. In the other cases, the difference to the average score remains below 1 point of

**Table 2** Adjusted Rand index of the run with lowest  $\mathcal{L}_{sp}$ , the average run and the best run. Score larger than the average are marked in boldface.

Criterion	MNIST			fMNIST			USPS			CIFAR10		
	$\mathcal{L}_{sp}$	Avg.	Best									
CM <sup>r</sup>	<b>42.7</b>	39.7	43.5	<b>44.2</b>	42.3	44.6	<b>54.8</b>	54.3	58.6	<b>4.8</b>	4.79	5.07
CM <sup>p</sup>	<b>43.3</b>	39.1	43.5	<b>44.0</b>	41.4	44.7	<b>55.8</b>	53.4	59.2	<b>4.94</b>	4.94	5.22
Criterion	R10K			20News			10x73k			Pendigit		
	$\mathcal{L}_{sp}$	Avg.	Best									
CM <sup>r</sup>	<b>56.0</b>	38.5	56.0	<b>9.92</b>	9.74	10.9	54.3	54.8	57.4	57.0	57.3	60.5
CM <sup>p</sup>	<b>62.9</b>	32.6	62.9	13.1	16.3	22.0	54.9	55.4	62.4	56.4	57.3	60.1

ARI expect for CM<sup>p</sup> on 20News. The average absolute difference with the best score is 1.60 and 3.10 for CM<sup>r</sup> and CM<sup>p</sup>, respectively. Without 20News, on which CM<sup>p</sup> performs the worst, that average difference drops to 2.25 for CM<sup>p</sup>. These are satisfying results that substantiates our heuristic that  $\mathcal{L}_{sp} = E_2 + E_3$  can be used as an internal metric for the CM.

## 5 The Clustering Network

The rationale of the clustering module goes beyond approximating  $k$ -means with a neural network. It was built to provide the foundations for a clustering model that is capable of non-linear partitions while maintaining a high level of interpretability thanks to the centroids.

### 5.1 Motivation and definition

The theory behind GMMs limits CM to a linear decoder, thus to a linear partition of the input space. Also the isotropy assumption, specific to CM, bars clusters to spread differently. We alleviate both *limitations* using a similar approach to that of kernel methods [18]: we project the input into a feature space where it will be clustered. However, we do not learn the kernel matrices but the feature maps using a deep autoencoder (DAE).

The idea is to optimize the CM and the DAE simultaneously, in order to let the latter find distortions of the input space along the way that guides the CM toward a better optima. Using a deep autoencoder architecture prevents the optimization to produce degenerate feature maps [17]. It also preserves the generative nature of the model: points in the input space can be generated from a mixture of centroids

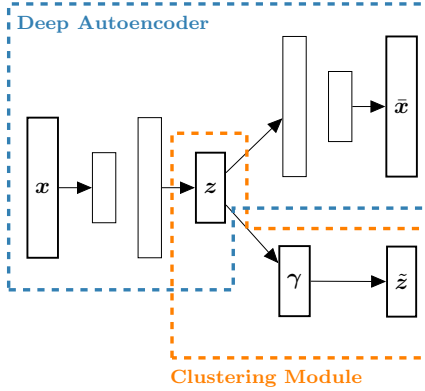


**Fig. 2** The proposed Clustering Network (C-Net) combines a deep autoencoder with a clustering module (CM).

in the feature space. We refer to this model as *Clustering Network* (C-Net). The architecture is illustrated in Figure 2. A clustering network consist of a clustering module nested into a deep autoencoder (Figure 2). The first part of the DAE encodes an input  $\mathbf{x} \in \mathbb{R}^d$  into a vector  $\mathbf{z} \in \mathbb{R}^p$ . Note, CM now works on code representation  $\mathbf{z}$  and not directly on the input  $\mathbf{x}$ .  $\mathbf{z}$  is fed to the CM and to the decoder of the DAE, yielding two outputs:  $\tilde{\mathbf{z}}$ , the CM’s reconstruction of  $\mathbf{z}$ , and  $\bar{\mathbf{x}}$ , the DAE’s reconstruction of  $\mathbf{x}$ .

### 5.1.1 Helping clustering with orthonormality

Empirical evaluation showed that current GD optimizers (e.g., Adam [24]) often return sub-optimal solutions when the reconstruction of the deep autoencoder is simply added to the loss of the CM. To help the optimization to find better optima, we add the assumption that the centroids are orthonormal:

$$\forall k, l, \boldsymbol{\mu}_k^T \boldsymbol{\mu}_l = \delta_{kl} = \begin{cases} 1 & \text{if } k = l, \\ 0 & \text{otherwise.} \end{cases} \quad (12)$$

Although the previous formula involves only  $\boldsymbol{\mu}$  which is learned by the nested clustering module, it affects the surrounding DAE. Indeed, the constraint encourages it to produce an embedding where the centroids can simultaneously be orthonormal and minimize CM’s loss. As a consequence,  $E_2$  simplifies and  $E_3$  becomes null:

$$\begin{aligned} E_2 &= \sum_{i=1}^N \sum_{k=1}^K \gamma_{ik} (1 - \gamma_{ik}) \|\boldsymbol{\mu}_k\|^2 = \sum_{i=1}^N \sum_{k=1}^K \gamma_{ik} (1 - \gamma_{ik}) \\ E_3 &= \sum_{i=1}^N \sum_{k=1}^K \sum_{\substack{l=1 \\ l \neq k}}^K \gamma_{ik} \gamma_{il} \boldsymbol{\mu}_k^T \boldsymbol{\mu}_l = 0 \end{aligned} \quad (13)$$

We employ Lagrange multipliers to integrate the orthonormality constraint. That way the final loss can be stated as follows:

$$\begin{aligned} \mathcal{L}_{\text{C-Net}}(\mathcal{X}; \Theta) &= \beta \sum_{i=1}^N \|\mathbf{x}_i - \bar{\mathbf{x}}_i\|^2 && \text{(Reconstruction DAE)} \\ &+ \sum_{i=1}^N \|\mathbf{z}_i - \tilde{\mathbf{z}}_i\|^2 && \text{(Reconstruction CM)} \\ &+ \sum_{i=1}^N \sum_{k=1}^K \gamma_{ik} (1 - \gamma_{ik}) && \text{(Sparsity)} \\ &+ \sum_{k=1}^K (1 - \alpha_k) \log(\tilde{\gamma}_k) && \text{(Dirichlet Prior)} \\ &+ \lambda \|\boldsymbol{\mu}^T \boldsymbol{\mu} - \mathbf{I}_K\|_1, && \text{(Orthonormality)} \end{aligned} \quad (14)$$

where  $\lambda > 0$  is the Lagrange multiplier and  $\beta > 0$  weights the DAE’s reconstruction loss. We choose the  $\ell_1$ -norm to enforce orthonormality, however other norms can be used.

Note that if the dimension of the embedding ( $p$ ) is larger than the number of centroids ( $K$ ), the embedding can always be transformed to satisfy the orthonormality of the centroids. On the other hand, if  $K > p$ , the assumption becomes restrictive also in term of possible clusterings. Nevertheless, its importance can be reduced with a small  $\lambda$ . This assumption also helps to avoid the centroids to collapse as their norm is required to be 1. An analysis of the Lagrange multiplier is provided in Appendix B.1.

The loss function of C-Net depends on four hyper-parameters: the weight  $\beta > 0$ , the concentration  $\alpha \in \mathbb{S}^K$ , the Lagrange multiplier  $\lambda > 0$  and the size of the batches  $B \in \mathbb{N}^*$ .

### 5.1.2 Implementation details

Since C-Net builds upon CM, any implementation also contains an averaging epoch (Section 4.2). In case of pre-training, both sub-networks need to be initialized. We favor a straightforward end-to-end training of the DAE (without drop-out or noise) over a few epochs. The clustering module is then initialized using  $k$ -means++ on the embedded data-set. Finally, the CM is optimized alone using  $\mathcal{L}_{\text{CM}}$  for a few epochs.

## 5.2 Empirical evaluation of the clustering network

In this section, we compare the clustering performance of our clustering network against a set of baselines empirically. Similarly to the CM, we propose a model selection scheme for C-Net leveraging the ambiguity of the assignments. We also evaluate the quality of the embeddings through the  $k$ -means clusterings thereof. Finally, we review the generative capabilities of our model.

### 5.2.1 Experimental setting

We use similar experimental setting as for CM and use the same data-sets (see Section A.5).

*Baselines and Implementations* The Clustering Network is implemented using TensorFlow 2.1 [3]<sup>4</sup>. We select the four standard baselines reviewed in Section 2: DEC [42], its extension IDEC [17], DCN [43] and DKM [13]. With the implementations of the first three being outdated, we re-implement them, while we for DKM use the implementation provided by the authors<sup>5</sup>. We also include as baseline, AE+KM, consisting of a trained DAE followed by  $k$ -means on the embedding.

We used the same architectures for all models. Following the settings used in [42, 17, 13], the encoder of the DAE consists of four fully-connected layers  $d - 500 - 500 - 2000 - p$  [21], where  $d$  represents the input dimension and  $p$  that of the feature space. The decoder mirrors the encoder. All activation functions

<sup>4</sup> Code available at:

<https://anonymous.4open.science/r/160597dc-005c-43bd-b5b3-3689e2bac054>

<sup>5</sup> <https://github.com/MaziarMF/deep-k-means>

(except the last one) are leaky-ReLU with a slope of 0.2, except for DKM for which the implementation requires ReLU.

The same Adam [24] optimizer (learning rate = 0.001,  $\beta_1 = 0.99$ ,  $\beta_2 = 0.999$ ,  $\epsilon = 10^{-3}$ ) is used for pre-training and training of all models but DKM. For USPS, CIFAR10, R10K, 10x73k and Pendigit, we use a polynomial decay on the learning rate from 0.001 to 0.0001 over 150 epochs. For DKM,  $\beta_1 = 0.9$  and  $\epsilon = 10^{-7}$ .

In case of random initialization, all the models but AE+KM are trained for 1,000 epochs. The pre-training is as follows: First AE+KM is trained in an end-to-end manner for 100 epochs. The resulting trained DAE is then used to initialize the other models' DAE. That way, all the pre-trained models start with same embedding. For C-Net, the nested clustering module is trained for 100 epochs before training the full model. Regarding DKM, we followed the setting of the original paper: DKM<sup>r</sup> includes the annealing of the softmax parameter updated every 5 epoch. The precise values of the hyper-parameters for each data-set and models are given in Table 8 of Appendix B.2.

### 5.2.2 Clustering performance

We repeat the same experimental setting as in Section 4.3 and compare clustering performances as well as initialization schemes for C-Net and its baselines.

Random and pre-trained initialization are indicated with <sup>r</sup> and <sup>p</sup>, respectively. Each experiment is repeated 20 times. We reports average ARI, NMI and ACC over 20 runs in Table 3. The scores non-statistically significant different from the highest on each data-set ( $p < .05$ ) are marked in boldface. A failure (–) corresponds to an average ARI close to 0. The \* indicate the model with the highest best score. An extended table including standard deviations and best run can be found in Table 10 of Appendix B.3.

In their original papers, the DEC, IDEC and DCN are pre-trained (<sup>p</sup>). We report here slightly lower scores that we impute to our implementation and slightly different architectures. However, the take-home message here is the consistency of their poor results when randomly initialized that reflects an inability to produce cluster from scratch, regardless of implementation. Note that, in that case, even  $k$ -means outperforms all of them on all the data-sets (see Table 1). On the other hand, DKM does return competitive score for both initialization scheme. Such results yield the question of how much clustering is performed by DEC, IDEC and DCN and how much is due to the pre-training phase?

In practice, DKM has proven sensitive to the choice of its  $\lambda$  hyper-parameter and to the duration of the optimization. For example, we could not find a value able to cluster Pendigit. We conjecture that expanding, as we did, the clustering term of DKM's loss would improve the robustness of the model.

On six of the data-sets, at least one of the variants of C-Net reports the highest average or highest best run. Especially, C-Net<sup>r</sup> produces competitive clusterings on all data-sets except CIFAR10 despite its random initialization. Also C-Net<sup>r</sup> always surpasses AE+KM except on R10K and CIFAR10, and even outperforms all the competitors by at least 20 ARI points on 20News. Assuming CM equivalent to  $k$ -means, this means that the embeddings produced by C-Net<sup>r</sup> are better suited to a  $k$ -means clustering than a DAE trained end-to-end. On the down side, C-Net<sup>r</sup> is associated with large standard deviations which implies a less predictable

**Table 3** The clustering scores ( $\times 100$ ) of different models on the selected data-sets. The highest score per column and those non-statistically different are marked in boldface. The – indicate failures. The \* indicate the model with the highest best score.

Model	MNIST			fMNIST			USPS			CIFAR10		
	ARI	NMI	ACC									
AE+KM	65.6	71.5	78.6	39.0	55.6	53.0	57.1	64.6	67.5	3.2	6.5	18.9
DCN <sup>r</sup>	10.1	25.6	25.4	17.0	33.5	29.0	2.5	9.7	20.9	3.2	5.9	18.0
DCN <sup>p</sup>	75.6	<b>82.5</b>	83.1	38.6	57.1	53.1	59.9	70.3	68.6	–	–	–
DEC <sup>r</sup>	11.1	19.0	28.9	22.9	38.1	39.2	36.0	47.7	48.4	3.1	5.7	18.6
DEC <sup>p</sup>	73.8	79.0	83.1	41.9	58.6	54.8	<b>65.9</b>	<b>74.8*</b>	<b>73.3</b>	3.1	5.6	18.2
IDEC <sup>r</sup>	27.5	39.0	42.5	35.2	50.8*	48.1	26.3	38.0	40.9	2.2	3.6	14.0
IDEC <sup>p</sup>	74.9	80.1	83.4	<b>42.8</b>	<b>59.8</b>	55.4	65.5	74.3	72.8	4.2	7.4	20.2
DKM <sup>r</sup>	72.5	77.3	81.2	41.8	56.4	54.6	51.2	61.1	62.3	<b>5.8*</b>	<b>9.9*</b>	<b>21.3*</b>
DKM <sup>p</sup>	74.0	78.3	82.7	36.2	52.0	47.0	55.7	64.4	66.5	<b>5.9</b>	<b>10.0</b>	19.7
CNET <sup>r</sup>	<b>77.9*</b>	80.9*	<b>86.1*</b>	<b>43.8*</b>	55.7	<b>59.1*</b>	55.5*	65.0	65.9*	–	–	–
CNET <sup>p</sup>	<b>79.4</b>	<b>82.4</b>	<b>86.5</b>	<b>43.9</b>	56.8	<b>59.0</b>	59.0	68.6	66.8	–	–	–
Model	R10K			20News			10x73k			Pendigit		
	ARI	NMI	ACC									
AE+KM	61.0	56.8	74.5	11.3	27.4	24.8	54.3	72.5	64.4	56.2	67.9	72.9
DCN <sup>r</sup>	16.0	16.4	48.0	–	–	–	5.3	17.2	23.9	5.8	15.1	17.4
DCN <sup>p</sup>	<b>66.0*</b>	<b>61.2*</b>	<b>77.2*</b>	11.7	33.5	25.3	9.6	13.8	25.2	59.8	73.2	74.5
DEC <sup>r</sup>	13.6	14.8	45.2	3.2	7.8	10.0	31.4	43.5	46.3	35.8	53.4	45.7
DEC <sup>p</sup>	58.6	57.3	<b>74.7</b>	5.5	11.3	11.8	53.5	67.1	62.1	60.1	72.0	74.1*
IDEC <sup>r</sup>	7.7	10.3	43.9	–	–	–	33.7	46.5	44.4	34.5	52.1	43.1
IDEC <sup>p</sup>	60.1	56.4	74.6	5.9	12.6	12.0	60.1	75.9	66.5	59.9	72.1	74.1
DKM <sup>r</sup>	51.5	50.0	71.8	4.7	14.1	10.9	65.5	71.3	77.0	–	–	–
DKM <sup>p</sup>	61.0	58.2	<b>75.9</b>	20.9	39.2	34.3	38.1	55.4	51.6	–	–	–
CNET <sup>r</sup>	46.1	45.9	67.4	<b>31.5*</b>	<b>45.3*</b>	<b>43.8*</b>	73.1	79.0	80.4	<b>64.0</b>	<b>74.3</b>	<b>75.9</b>
CNET <sup>p</sup>	61.7	57.2	<b>75.3</b>	16.8	29.0	32.5	<b>82.3*</b>	<b>83.7*</b>	<b>89.4*</b>	<b>65.5*</b>	<b>76.0*</b>	<b>77.4</b>

optimization (see Table 10 of Appendix B.3). Therefore, we investigate an internal measure to select the best run.

### 5.2.3 CM’s ambiguity as model selection for C-Net

Similarly to the CM, we discuss here a model selection heuristic for C-Net. The rationale behind the use of a DAE is to have an encoding facilitating the objective of the clustering module. Hence, we propose to use the heuristic of CM (Section 4.3.3).

In Table 4, we report the ARI of the runs with the lowest  $\mathcal{L}_{sp}$  for each data-set. For comparison, we also report the average and best ARI. Selected scores greater than the average are marked in boldface.

Again, scores associated to the lowest  $\mathcal{L}_{sp}$  are better than the average more than half of the time. However, the criterion never finds the best run. The average

**Table 4** Adjusted Rand index of the run with lowest  $\mathcal{L}_{\text{sp}}$ , the average run and the best run. Scores larger than the average are marked in boldface.

Criterion	MNIST			fMNIST			USPS			CIFAR10		
	$\mathcal{L}_{\text{sp}}$	Avg.	Best									
C-Net <sup>r</sup>	<b>87.0</b>	77.9	88.6	40.9	43.7	48.9	<b>60.6</b>	55.5	69.7	<b>4.61</b>	4.41	5.17
C-Net <sup>p</sup>	<b>79.5</b>	79.4	80.3	37.3	43.1	48.4	<b>62.3</b>	59.0	65.3	<b>4.53</b>	3.98	4.53
Criterion	R10K			20News			10x73k			Pendigit		
	$\mathcal{L}_{\text{sp}}$	Avg.	Best									
C-Net <sup>r</sup>	<b>53.0</b>	46.1	64.5	<b>34.3</b>	31.5	38.7	72.8	73.1	85.6	<b>64.6</b>	64.0	69.5
C-Net <sup>p</sup>	<b>65.9</b>	61.7	66.4	14.6	16.8	21.2	79.9	82.3	86.9	<b>66.3</b>	65.5	70.5

absolute difference to the highest score is 6.6 and 4.2 ARI points for C-Net<sup>r</sup> and C-Net<sup>p</sup>, respectively. Except for C-Net<sup>p</sup> on fMNIST, selected scores worse than the average are so by less than 3 points. In summary, while  $\mathcal{L}_{\text{sp}}$  as a criterion does not necessarily select the best run, it is not far from the expected one. Most importantly, such a model selection scheme filters out the worst runs.

#### 5.2.4 Embeddings for $k$ -means

All baselines, including our model, aim to learn an embedding prone to a  $k$ -means clustering. We audit this claim by running  $k$ -means on the embeddings produced by the 20 runs with random initialization on the MNIST data-set computed for Table 3 and report the average ARI, NMI and ACC in Table 5.

The results clearly show the superiority of methods utilizing a joint optimization, i.e., DKM<sup>r</sup>+KM and our C-Net<sup>r</sup>+KM. Interestingly, the clusterings of DCN<sup>r</sup>+KM are here better than those of DCN<sup>r</sup>. This discrepancy is certainly due the moving average used to update the centroids.

**Table 5** Average clustering performance of  $k$ -means on different embeddings. The highest score and those non-statistically different to it ( $p > 0.05$ ) are marked in boldface.

	AE+KM	DCN <sup>r</sup> +KM	DEC <sup>r</sup> +KM	IDE <sup>r</sup> +KM	DKM <sup>r</sup> +KM	C-NET <sup>r</sup> +KM
ARI	65.6	64.5	11.1	27.5	<b>74.5</b>	<b>75.2</b>
NMI	71.5	71.1	19.0	38.9	<b>78.8</b>	<b>78.5</b>
ACC	78.6	76.2	28.9	42.5	<b>83.0</b>	<b>84.8</b>

We continue the analysis of the embeddings with UMAP [35] projections. Figure 3 depicts the projections of different embeddings of the same 2,000 data-points. Figure 3a represents the UMAP projection from the input space. For (3b), we used the best run of AE+KM. For consistency, we used that embedding for C-Net<sup>p</sup>. Hence, Figure 3 (c) does not show the best run C-Net<sup>p</sup>. Finally (3d) is based on the best run of C-Net<sup>r</sup>.

The projection of MNIST from the input space (3a) has two pairs of classes entangled: (3, 5) and (4, 9). The end-to-end training of the DAE (3b) successfully

isolates each class except for cluster 4 (dark pink) and cluster 9 (light blue) which stay grouped together although separable. C-Net<sup>p</sup> (3c) further contracts the cluster around the centroids found by AE+KM, but fails to separate 4 and 9. Remark that even the best run of C-Net<sup>p</sup> does not to correctly split the data points. The centroids for 4 and 9 in Figures 3b and c are in comparable positions: they align along the gap separating the true clusters. This suggests that the optimization of C-Net<sup>p</sup> did not move them much. This remark applies to the pre-trained baselines, as well. Lastly, C-Net<sup>r</sup> successfully produces homogeneous groups (3f). Remark that the original entanglements of the pairs (3, 5) and (4, 9) are suggested by the trails between the corresponding clusters.

The previous observations summarize into two insights on the behavior of C-Net. If C-Net starts with an embedding associated to a low reconstruction loss for the DAE, the optimization contracts the clusters which yields higher ARI scores. However, it is unable to move the centroids to reach another local optimum. Although C-Net<sup>r</sup> separates (4, 9), it also produces clusters more spread than those of C-Net<sup>p</sup>. The improved performances of the latter over AE+KM indicates that C-Net<sup>r</sup> would benefit from tighter groups.

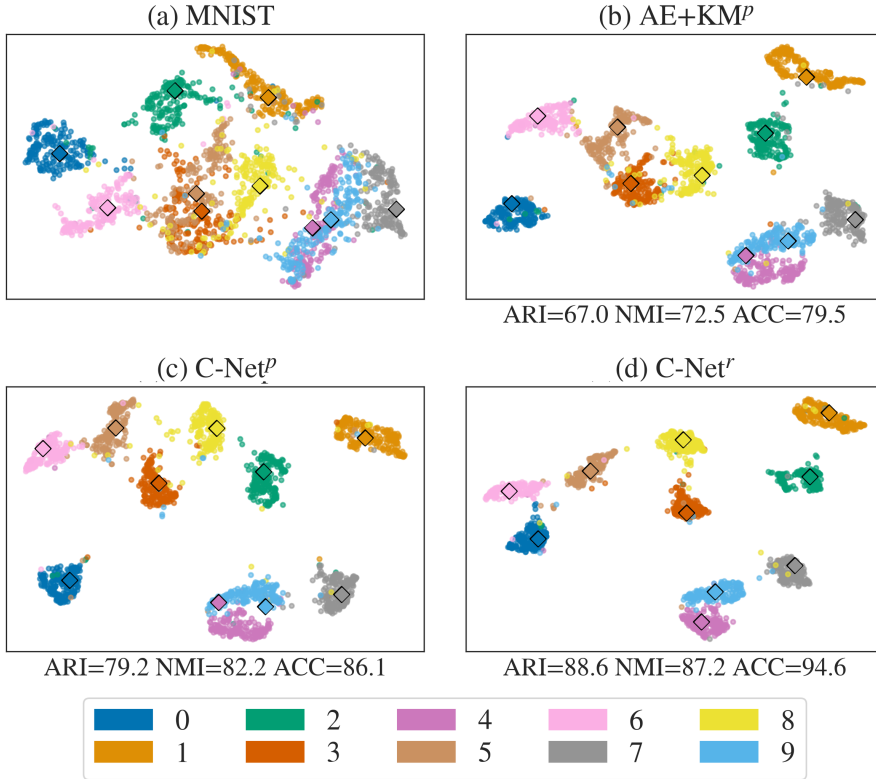


**Fig. 3** UMAP representation of a subset of MNIST and embeddings thereof learned by AE, IDEC and C-Net. The squares indicate the centroids.



**Fig. 4** Centroids mapped back to image space for AE+KM, IDEC<sup>p</sup>, DKM<sup>r</sup>, and C-Net<sup>r</sup>. The first row displays the average image of each class.

### 5.2.5 Sample generation and interpolation

Thanks to the reversible feature maps obtained by the DAE, both C-Net and its baselines (except DEC) are generative models. Figure 4 shows the decoding of the centroids of the best run of AE+KM (ARI=67.7), IDEC<sup>p</sup> (ARI=77.2), DKM<sup>r</sup> (ARI=83.6) and C-Net<sup>r</sup> (ARI=88.6). AE+KM's and IDEC<sup>p</sup>'s centroids for the 4 and 9 both look like 9's. With an ARI and an ACC larger than 80 and 90, respectively, DKM<sup>r</sup> and C-Net<sup>r</sup> both clustered the data correctly and found correct centroids for each class. Both models produce clear images for each class, which align reasonably well with the washed-out average image of the respective classes (first row).

Being a generative model, C-Net can also be used to interpolate between classes. Figure 5 shows a path made of nine interpolations between the ten centroids of C-Net<sup>r</sup>. We observe smooth transitions between all the pairs, which indicate that the model learned a smooth manifold from noise (random initialization).

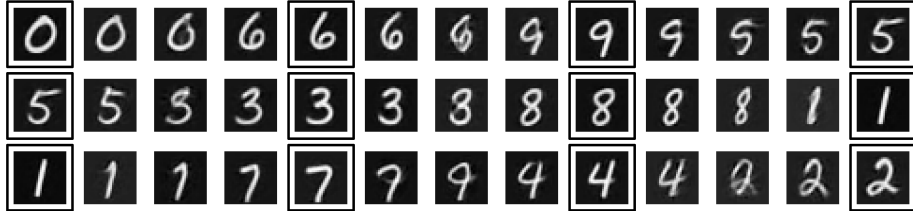


**Fig. 5** Linear interpolations between different centroids (plots with border) produced with C-Net.

## 6 Conclusion

We presented a novel clustering that is jointly optimized with the embedding of an autoencoder to allow for non-linear and interpretable clusterings. We first showed that the objective function of an isotropic GMM can be turned into a loss function

for autoencoders. The clustering module (CM) as the smallest resulting network was shown to perform similarly to  $k$ -means and GMM in extensive empirical evaluations. The module can be straight-forwardly incorporated into deep autoencoders to allow for non-linear clusterings. The resulting clustering network (C-Net) empirically outperformed existing centroid-based deep clustering architectures.

## References

1. 20 newsgroups dataset (empty). URL <http://people.csail.mit.edu/jrennie/20Newsgroups/>
2. Usps dataset (empty). URL <https://github.com/XifengGuo/IDEC/files/1613386/usps.zip>
3. Abadi, M., Barham, P., Chen, J., Chen, Z., Davis, A., Dean, J., Devin, M., Ghemawat, S., Irving, G., Isard, M., et al.: Tensorflow: A system for large-scale machine learning. In: 12th {USENIX} symposium on operating systems design and implementation ({OSDI} 16), pp. 265–283 (2016)
4. Alimoglu, F., Alpaydin, E.: Methods of combining multiple classifiers based on different representations for pen-based handwritten digit recognition. In: Proceedings of the fifth turkish artificial intelligence and artificial neural networks symposium (tainn 96). Citeseer (1996)
5. Arthur, D., Vassilvitskii, S.: k-means++: The advantages of careful seeding. In: Proceedings of the eighteenth annual ACM-SIAM symposium on Discrete algorithms, pp. 1027–1035. Society for Industrial and Applied Mathematics (2007)
6. Bezdek, J.C.: Pattern recognition with fuzzy objective function algorithms. Springer Science & Business Media (2013)
7. Bishop, C.M.: Pattern Recognition and Machine Learning (Information Science and Statistics). Springer-Verlag, Berlin, Heidelberg (2006)
8. Breiman, L., Friedman, J., Olshen, R., Stone, C.: Classification and Regression Trees. Wadsworth and Brooks, Monterey, CA (1984)
9. Dempster, A.P., Laird, N.M., Rubin, D.B.: Maximum likelihood from incomplete data via the em algorithm. *Journal of the Royal Statistical Society: Series B (Methodological)* **39**(1), 1–22 (1977)
10. Dhillon, I.S., Guan, Y., Kulis, B.: Kernel k-means: spectral clustering and normalized cuts. In: Proceedings of the tenth ACM SIGKDD international conference on Knowledge discovery and data mining, pp. 551–556 (2004)
11. Dunn, J.C.: A fuzzy relative of the isodata process and its use in detecting compact well-separated clusters (1973)
12. Estévez, P.A., Tesmer, M., Perez, C.A., Zurada, J.M.: Normalized mutual information feature selection. *IEEE Transactions on Neural Networks* **20**(2), 189–201 (2009)
13. Fard, M.M., Thonet, T., Gaussier, E.: Deep  $k$ -means: Jointly clustering with  $k$ -means and learning representations. *arXiv preprint arXiv:1806.10069* (2018)
14. Frandsen, P.B., Calcott, B., Mayer, C., Lanfear, R.: Automatic selection of partitioning schemes for phylogenetic analyses using iterative k-means clustering of site rates. *BMC evolutionary biology* **15**(1), 1–17 (2015)
15. Gasch, A.P., Eisen, M.B.: Exploring the conditional coregulation of yeast gene expression through fuzzy k-means clustering. *Genome biology* **3**(11), research0059–1 (2002)
16. Ghasedi Dizaji, K., Herandi, A., Deng, C., Cai, W., Huang, H.: Deep clustering via joint convolutional autoencoder embedding and relative entropy minimization. In: Proceedings of the IEEE international conference on computer vision, pp. 5736–5745 (2017)
17. Guo, X., Gao, L., Liu, X., Yin, J.: Improved deep embedded clustering with local structure preservation. In: International Joint Conference on Artificial Intelligence (IJCAI-17), pp. 1753–1759 (2017)
18. Guyon, I., Boser, B., Vapnik, V.: Automatic capacity tuning of very large vc-dimension classifiers. In: Advances in Neural Information Processing Systems, pp. 147–155. Morgan Kaufmann (1993)
19. Haeusser, P., Plapp, J., Golkov, V., Aljalbout, E., Cremers, D.: Associative deep clustering: Training a classification network with no labels. In: German Conference on Pattern Recognition, pp. 18–32. Springer (2018)

20. Hennig, C., Liao, T.F.: How to find an appropriate clustering for mixed-type variables with application to socio-economic stratification. *Journal of the Royal Statistical Society: Series C (Applied Statistics)* **62**(3), 309–369 (2013)
21. Hinton, G.E., Osindero, S., Teh, Y.W.: A fast learning algorithm for deep belief nets. *Neural computation* **18**(7), 1527–1554 (2006)
22. Hubert, L., Arabie, P.: Comparing partitions. *Journal of classification* **2**(1), 193–218 (1985)
23. Kampffmeyer, M., Løkse, S., Bianchi, F.M., Livi, L., Salberg, A.B., Jenssen, R.: Deep divergence-based approach to clustering. *Neural Networks* **113**, 91–101 (2019)
24. Kingma, D.P., Ba, J.: Adam: A method for stochastic optimization. In: International Conference on Learning Representations (2015)
25. Krishna, K., Murty, M.N.: Genetic k-means algorithm. *IEEE Transactions on Systems, Man, and Cybernetics, Part B (Cybernetics)* **29**(3), 433–439 (1999)
26. Krizhevsky, A., Hinton, G., et al.: Learning multiple layers of features from tiny images (2009)
27. Kuhn, H.W.: The hungarian method for the assignment problem. *Naval research logistics quarterly* **2**(1-2), 83–97 (1955)
28. Kulis, B., Jordan, M.I.: Revisiting k-means: new algorithms via bayesian nonparametrics. In: Proceedings of the 29th International Conference on International Conference on Machine Learning, pp. 1131–1138. Omnipress (2012)
29. LeCun, Y., Boser, B., Denker, J.S., Henderson, D., Howard, R.E., Hubbard, W., Jackel, L.D.: Backpropagation applied to handwritten zip code recognition. *Neural computation* **1**(4), 541–551 (1989)
30. Lewis, D.D., Yang, Y., Rose, T.G., Li, F.: Rcv1: A new benchmark collection for text categorization research. *Journal of machine learning research* **5**(Apr), 361–397 (2004)
31. Lloyd, S.: Least squares quantization in pcm. *IEEE transactions on information theory* **28**(2), 129–137 (1982)
32. Lücke, J., Forster, D.: k-means as a variational em approximation of gaussian mixture models. *Pattern Recognition Letters* **125**, 349–356 (2019)
33. Maaten, L.v.d., Hinton, G.: Visualizing data using t-sne. *Journal of machine learning research* **9**(Nov), 2579–2605 (2008)
34. McConville, R., Santos-Rodriguez, R., Piechocki, R.J., Craddock, I.: N2d:(not too) deep clustering via clustering the local manifold of an autoencoded embedding. arXiv preprint arXiv:1908.05968 (2019)
35. McInnes, L., Healy, J., Melville, J.: Umap: Uniform manifold approximation and projection for dimension reduction. arxiv 2018. arXiv preprint arXiv:1802.03426 (1802)
36. Mukherjee, S., Asnani, H., Lin, E., Kannan, S.: Clustergan: Latent space clustering in generative adversarial networks. In: Proceedings of the AAAI Conference on Artificial Intelligence, vol. 33, pp. 4610–4617 (2019)
37. Pedregosa, F., Varoquaux, G., Gramfort, A., Michel, V., Thirion, B., Grisel, O., Blondel, M., Prettenhofer, P., Weiss, R., Dubourg, V., Vanderplas, J., Passos, A., Cournapeau, D., Brucher, M., Perrot, M., Duchesnay, E.: Scikit-learn: Machine learning in Python. *Journal of Machine Learning Research* **12**, 2825–2830 (2011)
38. Punj, G., Stewart, D.W.: Cluster analysis in marketing research: Review and suggestions for application. *Journal of marketing research* **20**(2), 134–148 (1983)
39. Springenberg, J.T.: Unsupervised and semi-supervised learning with categorical generative adversarial networks. International Conference on Learning Representations (2016)
40. Wang, Z., Gu, Q., Ning, Y., Liu, H.: High dimensional em algorithm: Statistical optimization and asymptotic normality. In: Advances in neural information processing systems, pp. 2521–2529 (2015)
41. Xiao, H., Rasul, K., Vollgraf, R.: Fashion-mnist: a novel image dataset for benchmarking machine learning algorithms. arXiv preprint arXiv:1708.07747 (2017)
42. Xie, J., Girshick, R., Farhadi, A.: Unsupervised deep embedding for clustering analysis. In: International conference on machine learning, pp. 478–487 (2016)
43. Yang, B., Fu, X., Sidiropoulos, N.D., Hong, M.: Towards k-means-friendly spaces: Simultaneous deep learning and clustering. In: Proceedings of the 34th International Conference on Machine Learning-Volume 70, pp. 3861–3870. JMLR. org (2017)
44. Yang, J., Parikh, D., Batra, D.: Joint unsupervised learning of deep representations and image clusters. In: Proceedings of the IEEE Conference on Computer Vision and Pattern Recognition, pp. 5147–5156 (2016)
45. Zheng, G.X., Terry, J.M., Belgrader, P., Ryvkin, P., Bent, Z.W., Wilson, R., Ziraldo, S.B., Wheeler, T.D., McDermott, G.P., Zhu, J., et al.: Massively parallel digital transcriptional profiling of single cells. *Nature communications* **8**(1), 1–12 (2017)

## A Supplementary materials related to the clustering module

### A.1 CM: Hyper-parameters

The clustering module depends on two hyper-parameters: the size of the mini-batches and the concentration of the Dirichlet prior. To visualize their influence on the clustering performance, we trained a CM on Pendigit with various sizes of batch and concentrations. Figure 6 shows the variation of the final ARI score for both a random (left) and a  $k$ -means++ initialization (right). Both axes' scales are logarithmic: exponential base for the x-axis and base 10 for the y-axis. Each combination is run once. The ARI of each dot is the average of the nine neighboring combinations. Black dots indicate an average ARI greater than the ones reported in Table 1.

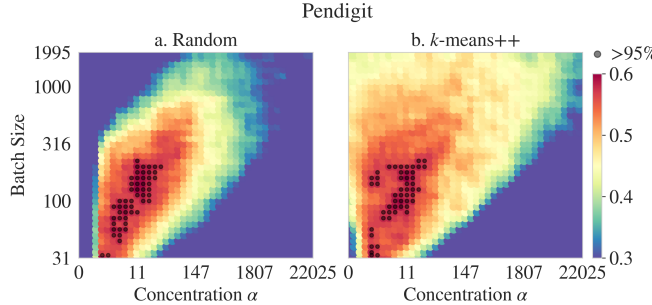


**Fig. 6** Clustering performance (ARI) for different combinations of batch-size, concentration and initialization scheme. Black dots indicate average ARI greater than the ones reported in Table 1.

There is a lower bound on  $\alpha$  under which the optimization of a randomly initialized model underperforms or fails. The  $k$ -means++ initialization removes this border and spreads out the well-performing area. The distribution in both settings means that the hyper-parameters can be tuned by fitting a bi-variate Gaussian distribution.

### A.2 CM: Non-symmetric prior

So far we considered only symmetric Dirichlet priors ( $\alpha = \alpha \mathbf{1}_K$ ,  $\alpha \in \mathbb{R}^+$ ) regardless of the imbalance between the labels. Here, we repeat the previous experiment using the true labels distribution as the prior, i.e.  $\alpha = \alpha \mathbf{f}$  where  $\mathbf{f} \langle f_k \rangle_K \in \mathbb{S}^K$  is the frequency of each label. In terms of implementation,  $E_4$  is computed by sorting both  $\alpha$  and  $\gamma_i$ . We evaluate results on the 10x73k and Pendigit data-sets, which have unbalance and balanced classes, respectively. We consider here only random initializations. Again, black dots indicate an average ARI greater than the ones reported in Table 1.

Figure 7b contains more black dots and a larger red area compared to 7a. The changes are greater than between Figure 7c and 6b. This discrepancy between the data-sets illustrates that unbalanced ones benefit more from a custom prior. However, a higher concentration is needed to enforce the distribution: the lower bound on  $\alpha$  is higher in Figure 7b and c than in 7a and 6a, respectively. Using the true class distribution, especially if the data is unbalanced, does ease the hyper-parameter selection. Nevertheless, such an information is not always known a priori.

### A.3 CM: Merging clusters with $E_3$

We claimed in Section 3.3 that  $E_3$  favors the merging of clusters. To illustrate this phenomenon, we train  $CM^r$  on the toy data-set of Section 4.2 with twice the number of true clusters (i.e.,

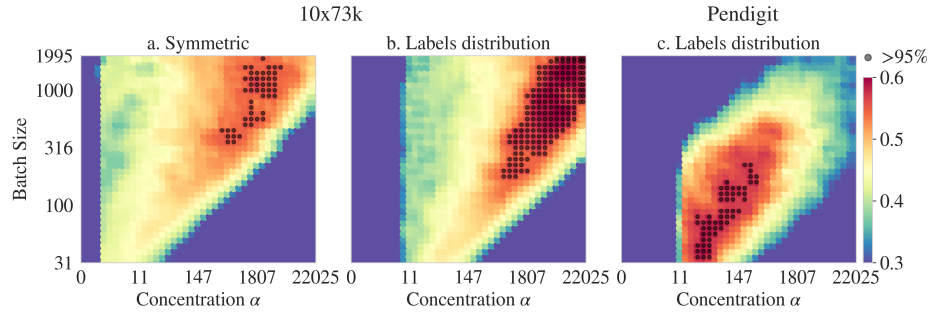


**Fig. 7** Clustering performance (ARI) for different combinations of batch-size, concentration and prior distribution. Black dots indicate average ARI greater than the ones reported in Table 1.

$K = 10$ ). We compare three variants of CM’s loss function: without  $E_3$ , with  $E_3$  and with  $E_3$  multiplied by 1.5. The final centroids and clustering are depicted in Figure 8. For legibility, overlapping centroids are slightly shifted using a Gaussian noise.

A vanilla CM (Figure 8b) correctly positions five pairs of centroids on top of the true cluster centroids. Without  $E_3$  (Fig. 8a), the model fails to merge the clusters properly. While five centroids are close to each of the true cluster, the five remaining are gathered around 0. Conversely, if  $E_3$  is weighted stronger (Fig. 8c), the model becomes so prone to merge clusters that it partitions the left cloud using only two groups of centroids.

#### A.4 CM: Clustering performance

Table 6 contains the full clustering results for CM, including standard deviation and the best run.

#### A.5 CM: Empirical setting

For the experiments reported in Section 4.3, the clustering module is trained over 150 epochs using the Adam optimizer (learning rate=0.001). The concentration  $\alpha$  and batch-size  $B$  used for each data-set are reported in Table 7. The hyper-parameters were optimized using Bayesian optimization over 2,000 iterations.

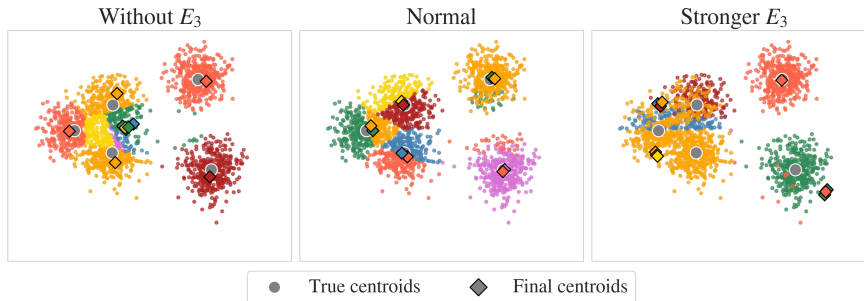


**Fig. 8** Final positions of the centroids depending on the importance of  $E_3$  in the loss of the clustering module.

## B Supplementary materials for C-Net

### B.1 C-Net: Hyper-parameters

Besides the architecture of the DAE, C-Net has two hyper-parameters more than CM:  $\beta$  weighting the reconstruction of the DAE and the Lagrange coefficient  $\lambda$  enforcing the orthonormality of the centroids. To visualize their influence on the clustering performance, a C-Net is trained on MNIST with various values of  $\beta$  and  $\lambda$ . Each combination is repeated five times. Note that

**Table 6** The clustering results of the methods on the experimental data-sets. The highest score per column and those non-statistically different are marked in boldface. Failures are indicated by  $-$ .

Model	MNIST			fMNIST			USPS			CIFAR10			
	ARI	NMI	ACC	ARI	NMI	ACC	ARI	NMI	ACC	ARI	NMI	ACC	
KM <sup>r</sup>	avg	37.8	<b>49.9</b>	54.5	36.6	51.6	53.2	52.6	<b>61.8</b>	63.0	4.2	8.1	20.8
	std	$\pm 2.7$	$\pm 1.9$	$\pm 4.3$	$\pm 1.7$	$\pm 1.2$	$\pm 3.4$	$\pm 2.3$	$\pm 1.4$	$\pm 3.2$	$\pm 0.1$	$\pm 0.2$	$\pm 0.4$
	max	43.4	<u>54.1</u>	<u>62.4</u>	38.5	53.1	59.4	56.2	63.9	68.3	4.3	8.3	21.7
KM <sup>p</sup>	avg	36.9	<b>49.2</b>	54.0	35.2	51.0	50.8	50.2	60.8	61.1	4.2	8.1	20.7
	std	$\pm 1.7$	$\pm 1.3$	$\pm 3.0$	$\pm 1.6$	$\pm 1.0$	$\pm 3.4$	$\pm 4.9$	$\pm 2.5$	$\pm 5.2$	$\pm 0.1$	$\pm 0.2$	$\pm 0.3$
	max	40.8	<u>52.1</u>	58.8	38.5	53.3	57.9	54.5	63.7	67.2	4.4	8.5	21.5
GMM <sup>r</sup>	avg	12.0	20.9	29.9	26.8	44.2	39.5	9.5	17.6	27.8	0.7	0.9	12.1
	std	$\pm 1.6$	$\pm 2.1$	$\pm 1.7$	$\pm 2.9$	$\pm 2.3$	$\pm 2.9$	$\pm 4.0$	$\pm 3.9$	$\pm 3.1$	$\pm 0.0$	$\pm 0.0$	$\pm 0.1$
	max	15.8	25.4	34.2	31.2	48.4	45.1	19.0	26.7	34.5	0.8	1.0	12.2
GMM <sup>p</sup>	avg	22.7	35.6	42.6	34.6	52.6	47.2	35.1	50.9	52.0	3.4	6.9	20.2
	std	$\pm 1.7$	$\pm 1.2$	$\pm 1.9$	$\pm 2.2$	$\pm 1.5$	$\pm 2.5$	$\pm 4.4$	$\pm 2.7$	$\pm 3.7$	$\pm 1.0$	$\pm 1.0$	$\pm 0.8$
	max	25.2	37.7	45.3	38.3	54.9	49.8	39.8	53.7	56.6	4.5	8.1	21.1
CM-EM <sup>r</sup>	avg	36.3	48.8	54.0	36.5	51.5	52.3	50.8	61.0	62.4	4.2	8.2	20.8
	std	$\pm 1.3$	$\pm 1.0$	$\pm 2.6$	$\pm 1.5$	$\pm 0.9$	$\pm 2.9$	$\pm 3.0$	$\pm 1.3$	$\pm 3.8$	$\pm 0.1$	$\pm 0.2$	$\pm 0.4$
	max	38.4	50.0	57.8	38.3	52.8	57.6	54.1	62.4	66.5	4.3	8.4	21.5
CM-EM <sup>p</sup>	avg	36.2	<b>49.2</b>	52.8	35.9	50.8	52.6	52.4	<b>61.8</b>	63.9	4.3	8.2	20.9
	std	$\pm 1.6$	$\pm 1.3$	$\pm 2.5$	$\pm 2.1$	$\pm 1.3$	$\pm 4.7$	$\pm 2.7$	$\pm 1.4$	$\pm 4.4$	$\pm 0.1$	$\pm 0.2$	$\pm 0.4$
	max	41.1	52.8	58.9	40.1	53.9	61.3	57.1	64.4	74.3	4.3	8.4	21.5
CM <sup>r</sup>	avg	<b>39.7</b>	<b>50.0</b>	<b>56.8</b>	<b>42.3</b>	<b>54.0</b>	<b>62.0</b>	<b>54.3</b>	<b>62.8</b>	<b>67.0</b>	4.8	8.9	<b>22.0</b>
	std	$\pm 1.9$	$\pm 1.5$	$\pm 2.1$	$\pm 3.4$	$\pm 2.3$	$\pm 4.1$	$\pm 2.1$	$\pm 1.0$	$\pm 2.5$	$\pm 0.2$	$\pm 0.3$	$\pm 0.5$
	max	43.5	53.0	60.8	44.6	55.7	64.4	58.6	65.1	75.0	5.1	9.4	23.2
CM <sup>p</sup>	avg	<b>39.1</b>	<b>49.5</b>	<b>55.9</b>	<b>41.4</b>	<b>53.4</b>	<b>60.7</b>	<b>53.4</b>	<b>62.8</b>	<b>63.7</b>	<b>4.9</b>	<b>9.3</b>	<b>22.3</b>
	std	$\pm 1.4$	$\pm 1.1$	$\pm 1.3$	$\pm 4.1$	$\pm 2.8$	$\pm 5.1$	$\pm 4.1$	$\pm 2.3$	$\pm 4.3$	$\pm 0.1$	$\pm 0.2$	$\pm 0.5$
	max	43.5	52.9	59.8	<u>44.7</u>	<u>55.8</u>	<u>64.5</u>	59.2	<u>66.9</u>	<u>69.6</u>	<u>5.2</u>	<u>9.7</u>	<u>23.2</u>
Model	R10K			20News			10x73k			Pendigit			
	ARI	NMI	ACC	ARI	NMI	ACC	ARI	NMI	ACC	ARI	NMI	ACC	
KM <sup>r</sup>	avg	<b>33.8</b>	<b>38.1</b>	<b>61.2</b>	14.8	<b>32.3</b>	<b>31.0</b>	36.5	55.4	55.0	<b>56.5</b>	67.8	<b>71.1</b>
	std	$\pm 14.3$	$\pm 10.2$	$\pm 11.9$	$\pm 1.3$	$\pm 1.9$	$\pm 1.9$	$\pm 0.8$	$\pm 0.7$	$\pm 1.8$	$\pm 3.7$	$\pm 1.9$	$\pm 4.8$
	max	61.5	56.4	80.3	17.4	36.1	34.5	37.3	56.1	56.3	62.3	70.6	76.8
KM <sup>p</sup>	avg	29.5	<b>36.0</b>	58.3	14.8	<b>33.5</b>	<b>32.0</b>	36.7	55.5	55.3	<b>58.1</b>	68.9	<b>72.7</b>
	std	$\pm 15.1$	$\pm 9.2$	$\pm 10.3$	$\pm 1.5$	$\pm 2.4$	$\pm 2.5$	$\pm 0.3$	$\pm 0.4$	$\pm 1.2$	$\pm 3.1$	$\pm 1.2$	$\pm 3.5$
	max	61.5	56.5	80.3	17.6	37.9	36.4	37.3	56.0	56.3	62.2	70.6	76.7
GMM <sup>r</sup>	avg	0.1	0.1	26.4	0.1	0.7	7.0	26.3	49.0	42.5	54.4	68.1	66.6
	std	$\pm 0.1$	$\pm 0.1$	$\pm 0.5$	$\pm 0.0$	$\pm 0.1$	$\pm 0.1$	$\pm 6.7$	$\pm 8.4$	$\pm 6.3$	$\pm 4.5$	$\pm 3.4$	$\pm 6.6$
	max	0.3	0.3	27.1	0.2	0.8	7.3	34.2	60.5	51.4	<u>63.2</u>	<u>74.9</u>	<u>79.0</u>
GMM <sup>p</sup>	avg	29.7	<b>36.2</b>	58.4	14.8	<b>33.5</b>	<b>32.0</b>	38.4	61.7	55.6	55.4	<b>70.1</b>	<b>71.5</b>
	std	$\pm 15.0$	$\pm 9.2$	$\pm 10.2$	$\pm 1.5$	$\pm 2.4$	$\pm 2.5$	$\pm 2.3$	$\pm 1.5$	$\pm 3.3$	$\pm 3.1$	$\pm 1.7$	$\pm 3.0$
	max	61.5	56.5	80.3	17.6	37.9	36.4	40.3	62.7	58.1	60.4	73.8	78.6
CM-EM <sup>r</sup>	avg	19.0	25.4	53.7	0.0	-0.0	5.3	10.1	19.1	29.7	0.0	-0.0	10.4
	std	$\pm 13.7$	$\pm 10.9$	$\pm 10.0$	$\pm 0.0$	$\pm 0.0$	$\pm 0.0$	$\pm 0.6$	$\pm 0.5$	$\pm 0.6$	$\pm 0.0$	$\pm 0.0$	$\pm 0.0$
	max	56.3	52.4	78.7	0.0	-0.0	5.3	10.6	20.0	30.3	0.0	-0.0	10.4
CM-EM <sup>p</sup>	avg	17.9	24.2	53.4	0.0	-0.0	5.3	12.3	27.7	33.8	0.0	-0.0	10.4
	std	$\pm 10.6$	$\pm 7.8$	$\pm 9.1$	$\pm 0.0$	$\pm 0.0$	$\pm 0.0$	$\pm 1.9$	$\pm 3.4$	$\pm 2.8$	$\pm 0.0$	$\pm 0.0$	$\pm 0.0$
	max	44.1	45.5	72.2	0.0	-0.0	5.3	15.1	29.9	37.1	0.0	-0.0	10.4
CM <sup>r</sup>	avg	<b>38.5</b>	<b>41.0</b>	<b>64.9</b>	9.7	21.2	18.3	<b>54.8</b>	<b>63.8</b>	<b>69.5</b>	<b>57.3</b>	67.0	<b>72.0</b>
	std	$\pm 10.6$	$\pm 7.1$	$\pm 8.1$	$\pm 0.7$	$\pm 0.7$	$\pm 0.8$	$\pm 1.2$	$\pm 0.6$	$\pm 2.0$	$\pm 1.7$	$\pm 1.2$	$\pm 2.5$
	max	56.0	55.2	76.4	10.9	22.6	20.0	57.4	65.2	74.3	60.5	69.1	76.4
CM <sup>p</sup>	avg	<b>32.6</b>	<b>39.2</b>	<b>60.2</b>	<b>16.3</b>	28.8	<b>30.8</b>	<b>55.4</b>	<b>64.0</b>	<b>71.0</b>	<b>57.3</b>	66.9	<b>72.3</b>
	std	$\pm 12.7$	$\pm 8.1$	$\pm 10.0$	$\pm 2.4$	$\pm 2.4$	$\pm 2.5$	$\pm 3.0$	$\pm 2.0$	$\pm 3.8$	$\pm 2.0$	$\pm 1.3$	$\pm 2.3$
	max	62.9	57.8	80.9	22.0	34.1	36.1	62.4	67.8	78.8	60.1	68.6	75.0

**Table 7** Hyper-parameters used for the experiments in Section 4.3.

	MNIST	fMNIST	USPS	CIFAR10	R10K	20News	10x73k	Pendigit
$\alpha$	177	80	40	164	10	11	1000	13
$B$	111	35	150	350	400	85	500	80

when  $\beta = 0$  the setting is equivalent to training only the encoder of the DAE (akin to DEC). Also, if  $\lambda = 0$  the orthogonality constraint is omitted. Figure 9 represents the average ARI scores for each combination and both initialization schemes as a heat-map.

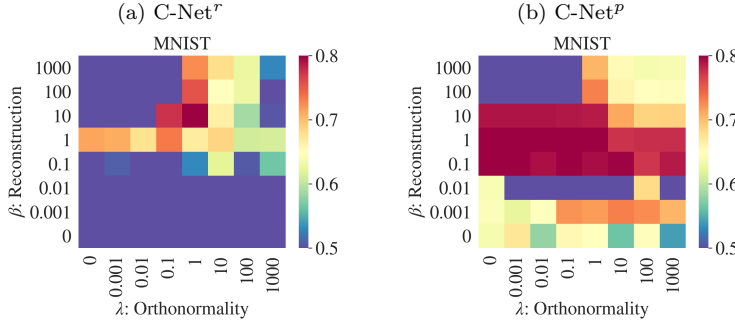


**Fig. 9** Clustering performance (ARI) of C-Net on MNIST for different values of  $\beta$  and  $\lambda$  and initialization scheme.

With a random initialization (Figure 9a), if both  $\beta$  and  $\lambda$  are not large enough, the clustering fails, excepted when  $\beta = 1$ . In that case, the model performs well for every value of  $\lambda$ , even for  $\lambda = 0$ , i.e., without the orthonormality constraint. Conversely, the C-Net<sup>r</sup> always fails if trained without the reconstruction of the DAE, ( $\beta = 0$ ) . As the order of magnitude of both parameters increases, the performances worsen.

The distribution of C-Net<sup>p</sup> (Figure 9b) presents similarities with the previous one. Overall the average performances are better for each combination. When  $\beta$  is very small, the ARI exceeds 0.5. The performance also decrease as  $\beta$  and  $\lambda$  become larger. Most noticeable, the band around  $\beta = 1$  is still there, but it is thicker. This is in line with the similar analysis on CM (Section A.1): Pre-trained models are less sensitive to hyperparameters.

## B.2 C-Net: Empirical setting

For the experiments reported in Section 5.2, the clustering network is trained over 150 epochs using the Adam optimizer (learning rate=0.001). Each layer of the DAE is activated with a leaky-ReLU with a slope of 0.2, except for the last one of the encoder and of the decoder. C-Net depends on four hyper-parameters: the weight  $\beta > 0$ , the concentration  $\alpha \in \mathbb{S}^K$ , the Lagrange multiplier  $\lambda > 0$  and the size of the batches  $B \in \mathbb{N}^*$ . The four hyper-parameters plus the dimension of the feature space,  $p$ ; were optimized using Bayesian optimization over 2,000 iterations. The selected values are reported in Table 8.

The same architecture is used for the baselines, except for DKM where the activation are all ReLU. DEC, IDEC and DCN update their clustering every  $u$  iterations, IDEC and DCN rely on a hyper-parameter  $\gamma$  and DKM on a  $\lambda$ . Regarding DKM, the annealing process of the softmax parameter is updated every 5 epochs. We report in Table 8 the values used for each data-set.

**Table 8** Hyper-parameters used to train C-Net for the experiments in Section 5.2.

	MNIST	fMNIST	USPS	CIFAR10	R10K	20News	10x73k	Pendigit
$\alpha$	230	13	3	64	1.7	10	7	13
$\beta$	5	47	0.04	1	2.3	232	15	0.5
$\lambda$	1.	1.	1.	1	1	1	1	1
$B$	500	175	45	256	250	300	7	80
$p$	10	10	30	10	75	100	10	70

**Table 9** Hyper-parameters used to train the baselines for the experiments in Section 5.2.

	MNIST	fMNIST	USPS	CIFAR10	R10K	20News	10x73k	Pendigit
$u$	140	140	30	140	20	20	20	20
$\gamma$	0.1	0.1	0.1	0.1	0.1	0.1	0.1	0.1
$\lambda^r$	0.1	0.01	0.01	0.01	0.01	$10^{-4}$	$10^{-4}$	$10^{-4}$
$\lambda^p$	1.0	0.01	0.1	0.1	1.0	0.01	$10^{-4}$	$10^{-4}$
$B$	256	256	256	256	256	256	256	256

### B.3 C-Net: Clustering performance

Table 10 contains the full clustering results for C-Net, including standard deviation and the best run.

**Table 10** Clustering performance of the methods on the experimental data-sets including average, standard deviation and best run. The highest score per column and those non-statistically different are marked in boldface. Highest best run is underscored. Failures are indicated by  $-$ .

Model	MNIST			fMNIST			USPS			CIFAR10			
	ARI	NMI	ACC	ARI	NMI	ACC	ARI	NMI	ACC	ARI	NMI	ACC	
AE+KM	avg	65.6	71.5	78.6	39.0	55.6	53.0	57.1	64.6	67.5	3.2	6.5	18.9
	std	$\pm 1.0$	$\pm 0.7$	$\pm 0.6$	$\pm 0.9$	$\pm 0.5$	$\pm 2.3$	$\pm 1.0$	$\pm 0.9$	$\pm 1.0$	$\pm 0.3$	$\pm 0.5$	$\pm 0.5$
	max	67.7	73.0	79.6	41.0	56.7	56.9	59.4	66.6	69.5	3.7	7.2	20.2
DCN <sup>r</sup>	avg	10.1	25.6	25.4	17.0	33.5	29.0	2.5	9.7	20.9	3.2	5.9	18.0
	std	$\pm 11.0$	$\pm 17.4$	$\pm 9.3$	$\pm 11.7$	$\pm 16.9$	$\pm 11.3$	$\pm 3.6$	$\pm 11.2$	$\pm 5.2$	$\pm 2.2$	$\pm 3.5$	$\pm 4.6$
	max	30.4	51.6	45.1	40.7	57.5	52.4	11.0	31.9	32.5	5.8	10.3	22.9
DCN <sup>p</sup>	avg	75.6	<b>82.5</b>	83.1	38.6	57.1	53.1	59.9	70.3	68.6	0.1	0.6	10.7
	std	$\pm 1.4$	$\pm 1.2$	$\pm 0.9$	$\pm 2.0$	$\pm 0.8$	$\pm 1.8$	$\pm 1.4$	$\pm 1.1$	$\pm 0.4$	$\pm 1.2$	$\pm 1.5$	
	max	77.6	85.0	84.5	41.7	58.6	56.4	62.6	72.4	70.3	1.3	4.0	14.5
DEC <sup>r</sup>	avg	11.1	19.0	28.9	22.9	38.1	39.2	36.0	47.7	48.4	3.1	5.7	18.6
	std	$\pm 2.6$	$\pm 3.2$	$\pm 3.6$	$\pm 3.9$	$\pm 4.1$	$\pm 4.2$	$\pm 5.3$	$\pm 4.6$	$\pm 4.2$	$\pm 0.9$	$\pm 1.5$	$\pm 1.4$
	max	16.7	24.1	36.6	29.7	47.0	47.0	44.6	55.6	54.5	4.7	8.6	21.7
DEC <sup>p</sup>	avg	73.8	79.0	83.1	41.9	58.6	54.8	<b>65.9</b>	<b>74.8</b>	<b>73.3</b>	3.1	5.6	18.2
	std	$\pm 0.7$	$\pm 0.4$	$\pm 0.5$	$\pm 2.0$	$\pm 1.9$	$\pm 2.2$	$\pm 0.8$	$\pm 0.6$	$\pm 0.6$	$\pm 1.4$	$\pm 2.4$	$\pm 3.6$
	max	75.2	79.5	84.1	45.9	60.6	58.4	68.0	76.3	75.0	4.5	7.8	21.8
IDE <sup>r</sup>	avg	27.5	39.0	42.5	35.2	50.8	48.1	26.3	38.0	40.9	2.2	3.6	14.0
	std	$\pm 5.0$	$\pm 5.2$	$\pm 4.8$	$\pm 5.1$	$\pm 5.6$	$\pm 5.9$	$\pm 9.9$	$\pm 10.2$	$\pm 7.3$	$\pm 2.3$	$\pm 3.6$	$\pm 3.9$
	max	38.3	50.1	50.2	48.4	62.5	62.5	39.4	52.5	53.0	5.3	9.3	20.4
IDE <sup>p</sup>	avg	74.9	80.1	83.4	<b>42.8</b>	<b>59.8</b>	55.4	65.5	74.3	72.8	4.2	7.4	20.2
	std	$\pm 1.0$	$\pm 0.6$	$\pm 0.6$	$\pm 1.8$	$\pm 0.7$	$\pm 2.2$	$\pm 0.5$	$\pm 0.5$	$\pm 0.4$	$\pm 0.4$	$\pm 0.7$	$\pm 1.1$
	max	77.2	81.3	84.9	47.0	61.3	59.2	67.0	75.7	73.6	4.9	8.5	22.0
DKM <sup>r</sup>	avg	72.5	77.3	81.2	41.8	56.4	54.6	51.2	61.1	62.3	<b>5.8</b>	<b>9.9</b>	<b>21.3</b>
	std	$\pm 5.0$	$\pm 3.1$	$\pm 5.0$	$\pm 2.2$	$\pm 0.9$	$\pm 3.3$	$\pm 3.4$	$\pm 2.9$	$\pm 3.1$	$\pm 0.7$	$\pm 1.2$	$\pm 2.1$
	max	83.6	83.5	92.3	46.0	58.6	59.4	55.8	65.5	68.6	7.1	12.6	24.3
DKM <sup>p</sup>	avg	74.0	78.3	82.7	36.2	52.0	47.0	$\pm 55.7$	64.4	66.5	<b>5.9</b>	<b>10.0</b>	19.7
	std	$\pm 2.8$	$\pm 1.7$	$\pm 3.0$	$\pm 3.0$	$\pm 2.3$	$\pm 3.7$	$\pm 3.5$	$\pm 1.9$	$\pm 3.4$	$\pm 0.4$	$\pm 0.6$	$\pm 1.2$
	max	76.9	80.2	85.3	40.5	56.3	51.5	60.4	66.3	72.9	6.2	10.8	20.8
CNET <sup>r</sup>	avg	<b>77.9</b>	80.9	<b>86.1</b>	<b>43.7</b>	55.6	<b>59.2</b>	55.5	65.0	65.9	4.3	7.7	<b>20.7</b>
	std	$\pm 4.0$	$\pm 2.4$	$\pm 3.2$	$\pm 2.9$	$\pm 1.8$	$\pm 3.5$	$\pm 6.7$	$\pm 5.0$	$\pm 6.4$	$\pm 0.6$	$\pm 1.1$	$\pm 1.2$
	max	88.6	87.2	94.6	48.9	58.5	65.6	69.7	76.2	75.6	5.2	9.1	22.3
CNET <sup>p</sup>	avg	<b>79.4</b>	<b>82.4</b>	<b>86.5</b>	<b>43.1</b>	56.3	<b>58.5</b>	59.0	68.6	66.8	4.3	8.0	<b>20.6</b>
	std	$\pm 0.4$	$\pm 0.4$	$\pm 0.4$	$\pm 2.6$	$\pm 1.7$	$\pm 2.8$	$\pm 4.6$	$\pm 2.9$	$\pm 4.6$	$\pm 0.6$	$\pm 1.2$	$\pm 0.8$
	max	80.3	83.2	87.3	48.4	58.5	64.9	65.3	73.1	74.1	4.9	9.3	21.4
Model	R10K			20News			10x73k			Pendigit			
	ARI	NMI	ACC	ARI	NMI	ACC	ARI	NMI	ACC	ARI	NMI	ACC	
AE+KM	avg	61.0	56.8	74.5	11.3	27.4	24.8	54.3	72.5	64.4	56.2	67.9	72.9
	std	$\pm 3.5$	$\pm 3.1$	$\pm 3.3$	$\pm 1.6$	$\pm 2.5$	$\pm 2.5$	$\pm 6.6$	$\pm 3.0$	$\pm 4.8$	$\pm 2.6$	$\pm 1.4$	$\pm 3.6$
	max	67.3	62.2	83.3	13.8	31.0	28.6	64.5	78.3	72.4	62.7	71.5	78.1
DCN <sup>r</sup>	avg	16.0	16.4	48.0	0.0	0.2	5.6	5.3	17.2	23.9	5.8	15.1	17.4
	std	$\pm 8.5$	$\pm 6.8$	$\pm 7.1$	$\pm 0.1$	$\pm 0.3$	$\pm 0.5$	$\pm 6.9$	$\pm 16.7$	$\pm 7.2$	$\pm 5.1$	$\pm 11.3$	$\pm 5.0$
	max	33.0	34.7	60.8	0.3	0.9	6.8	26.6	52.3	38.9	12.5	27.2	21.8
DCN <sup>p</sup>	avg	<b>66.0</b>	<b>61.2</b>	<b>77.2</b>	11.7	33.5	25.3	9.6	13.8	25.2	<b>59.8</b>	73.2	74.5
	std	$\pm 2.6$	$\pm 2.4$	$\pm 3.0$	$\pm 2.0$	$\pm 2.8$	$\pm 2.8$	$\pm 22.0$	$\pm 27.3$	$\pm 18.6$	$\pm 4.2$	$\pm 1.5$	$\pm 5.0$
	max	69.4	63.4	84.1	16.1	37.4	30.4	65.8	80.4	72.4	64.9	75.8	78.9
DEC <sup>r</sup>	avg	13.6	14.8	45.2	3.2	7.8	10.0	31.4	43.5	46.3	35.8	53.4	45.7
	std	$\pm 5.9$	$\pm 5.9$	$\pm 5.8$	$\pm 0.9$	$\pm 2.2$	$\pm 1.1$	$\pm 8.6$	$\pm 9.6$	$\pm 8.1$	$\pm 4.8$	$\pm 4.6$	$\pm 4.6$
	max	25.5	26.3	56.6	4.3	10.6	10.7	53.1	66.3	68.4	42.2	59.6	53.4
DEC <sup>p</sup>	avg	58.6	57.3	<b>74.7</b>	5.5	11.3	11.8	53.5	67.1	62.1	60.1	72.0	74.1
	std	$\pm 3.9$	$\pm 3.7$	$\pm 4.8$	$\pm 0.6$	$\pm 1.3$	$\pm 0.3$	$\pm 18.6$	$\pm 22.8$	$\pm 15.9$	$\pm 4.1$	$\pm 2.4$	$\pm 4.1$
	max	65.5	62.7	83.3	6.5	13.7	12.2	73.3	83.4	78.5	68.7	76.9	81.1
IDE <sup>r</sup>	avg	7.7	10.3	43.9	0.0	0.1	5.5	33.7	46.5	44.4	34.5	52.1	43.1
	std	$\pm 4.5$	$\pm 4.3$	$\pm 5.0$	$\pm 0.0$	$\pm 0.3$	$\pm 0.4$	$\pm 11.6$	$\pm 12.9$	$\pm 8.5$	$\pm 5.2$	$\pm 5.9$	$\pm 5.5$
	max	14.6	17.2	52.2	0.1	1.1	6.7	67.5	82.8	69.6	45.3	61.9	55.0
IDE <sup>p</sup>	avg	60.1	56.4	74.6	5.9	12.6	12.0	60.1	75.9	66.5	59.9	72.1	74.1
	std	$\pm 3.0$	$\pm 2.8$	$\pm 3.4$	$\pm 0.4$	$\pm 1.2$	$\pm 0.2$	$\pm 4.9$	$\pm 4.0$	$\pm 3.9$	$\pm 3.5$	$\pm 2.0$	$\pm 4.1$
	max	65.8	61.4	82.7	6.6	15.0	12.4	73.4	83.5	78.8	65.5	74.7	78.9
DKM <sup>r</sup>	avg	51.5	50.0	71.8	4.7	14.1	10.9	65.5	71.3	77.0	0.0	0.0	0.0
	std	$\pm 3.4$	$\pm 2.8$	$\pm 2.3$	$\pm 0.9$	$\pm 2.5$	$\pm 1.1$	$\pm 5.1$	$\pm 3.7$	$\pm 5.0$	$\pm 0.0$	$\pm 0.0$	$\pm 0.0$
	max	59.5	54.6	77.7	5.6	17.8	13.0	77.0	78.5	88.1	0.0	0.0	0.0
DKM <sup>p</sup>	avg	61.0	58.2	<b>75.9</b>	20.9	39.2	34.3	38.1	55.4	51.6	0.0	0.0	0.0
	std	$\pm 1.7$	$\pm 0.9$	$\pm 1.5$	$\pm 6.5$	$\pm 5.3$	$\pm 6.9$	$\pm 14.6$	$\pm 11.4$	$\pm 10.2$	$\pm 0.0$	$\pm 0.0$	$\pm 0.0$
	max	63.6	59.7	78.4	30.7	46.7	44.0	57.2	69.2	63.6	0.0	0.0	0.0
CNET <sup>r</sup>	avg	46.1	45.9	67.4	<b>31.5</b>	<b>45.3</b>	<b>43.3</b>	73.1	79.0	80.4	<b>64.0</b>	<b>74.3</b>	<b>75.9</b>
	std	$\pm 11.4$	$\pm 8.4$	$\pm 7.5$	$\pm 4.6$	$\pm 3.3$	$\pm 4.1$	$\pm 5.9$	$\pm 3.7$	$\pm 5.4$	$\pm 4.9$	$\pm 3.2$	$\pm 3.9$
	max	64.5	57.4	81.4	38.7	50.8	50.5	85.6	86.2	92.1	69.5	78.4	80.7
CNET <sup>p</sup>	avg	61.7	57.2	<b>75.3</b>	16.8	29.0	32.5	<b>82.3</b>	<b>83.7</b>	<b>89.4</b>	<b>65.5</b>	<b>76.0</b>	<b>77.4</b>
	std	$\pm 3.0$	$\pm 2.6$	$\pm 3.2$	$\pm 2.5$	$\pm 2.7$	$\pm 2.9$	$\pm 5.7$	$\pm 3.4$	$\pm 5.0$	$\pm 3.1$	$\pm 2.1$	$\pm 2.9$
	max	66.4	60.6	82.4	21.2	33.5	37.8	86.9	86.8	92.9	70.5	79.3	80.8